

# Effect of the long-range interaction in transport through one-dimensional nanoparticle arrays

E. Bascones<sup>1,2,3,\*</sup>, J.A. Trinidad<sup>2</sup>, V. Estévez<sup>1</sup> and A.H. MacDonald<sup>2</sup>

<sup>1</sup>*Instituto de Ciencia de Materiales de Madrid, CSIC, Cantoblanco, E-28049 Madrid, Spain*

<sup>2</sup>*Department of Physics, University of Texas at Austin, Austin TX-78712, USA*

<sup>3</sup>*Theoretische Physik, ETH-Hönggerberg, CH-8050 Zurich, Switzerland\**

(Dated: September 12, 2021)

We analyze the effect of the long-range interaction on the transport properties through ordered and disordered one-dimensional metallic nanoparticle arrays. We discuss how the threshold voltage, the I-V curves and the voltage drop through the array are modified as compared to the case in which interactions are restricted to charges placed on the same island. We show that some of these modifications are due to finite interactions between charges in different nanoparticles while other ones are due to interactions between charges in the islands and those at the electrodes, what produces a polarization potential drop through the array. We study the screening of the disorder potential due to charged impurities trapped in the substrate and find that long-range interactions introduce correlations between the disorder potentials of neighboring islands.

PACS numbers: 73.23.-b, 73.63.-b, 73.23.Hk

## I. INTRODUCTION

Nanoparticle arrays<sup>1,2,3,4,5,6,7,8,9,10,11,12,13,14,15,16,17,18,19,20,21,22</sup> are a perfect system to analyze correlated electronic transport and have received a lot of experimental and theoretical attention during the last decade<sup>23,24,25,26,27,28,29,30,31,32,33,34,35,36,37,38,39,40,41,42,43,44,45,46,47,48,49,50</sup>. In spite of this, their properties and I-V characteristics are not well understood. The presence of disorder in these arrays complicates the analysis<sup>48,49,50</sup>. The two most relevant and experimentally unavoidable types of disorder are charging disorder due to random charges quenched at the substrate and resistance disorder due to small changes in the distance between the nanoparticles and the exponential dependence of the resistance on the distance. Voids in the lattice or a non-homogeneous distribution of nanoparticle size can be also present<sup>3</sup> but this source of disorder is less important in some recent experiments.

Theoretical analysis have mainly considered arrays in which each nanoparticle is capacitively coupled only to its nearest neighbors<sup>33,34,39,51,52,53,54</sup>, especially the case in which this coupling is small. The truncation of capacitive coupling to nearest neighbor results in an interaction between charges in different conductors which decays exponentially with the distance between them<sup>33,34</sup>. This limit is relevant for those arrays coupled to a gate electrode<sup>55</sup>, as the mobile charges in this lead effectively screen Coulomb interactions. A complete description of the non-equilibrium transport through arrays has been presented only very recently<sup>56</sup> and is restricted to one-dimensional metallic nanoparticle arrays in which interactions are finite only when charges are placed on the same conductor.

Self-assembled arrays fabricated nowadays are deposited onto insulating substrates and generally lack a gate voltage. In these arrays, the screening of long-range interactions is less effective, but the proximity of other

conductors, both islands and leads, modifies its value compared to a  $1/r$  Coulomb law<sup>57,58</sup>. The electrodes contribute to the screening of the interaction. Theoretical analysis including the effect of long-range interactions are scarce and limited<sup>39,41,59</sup> to numerical results or particular cases. In this paper we perform a detailed analysis of the effect of the long-range character of the interaction on the transport properties through ordered and disordered one-dimensional arrays. We consider the influence of charging and resistance disorder. The interactions are described by an inverse capacitance matrix, in which coupling to other conductors is not truncated. The matrix is calculated including the effect of screening and the current is computed numerically. Some analytical approximations are also discussed and compared with the numerical results. This comparison allows us to understand the origin of the behavior found. To analyze the transport we put forward a model to describe the electrostatic interactions among the charges occupying the islands and the electrodes, which allows for a clear description of the relevant contributions to the transport. In particular, we introduce the concept of polarization potential drop at the junctions between the nanoparticles. As in our previous study of the short-range case<sup>56</sup>, we analyze the threshold voltage, flow of current and voltage drop for the cases with and without charge or junction resistance disorder.

The organization of the paper is as follows. Section II describes the system under study and the model used to analyze the transport properties and compares it with previous models used in the literature. In section III we discuss the correlations introduced by the long-range character of the interaction in the disorder potential. Section IV, V and VI respectively analyze the threshold voltage, I-V characteristics and voltage drop through the array. In section VII we summarize our results. Finally, in Appendix I we describe the two methods employed to calculate the screened interaction between charges, and

in Appendix II we discuss the effect of screening on the distance-dependence of this interaction.

## II. THE MODEL

We consider an array composed of  $N$  metallic spheres of radius  $r^{isl}$  and center to center distance  $2r^{isl} + d$ . Throughout lengths are measured in units of  $r^{isl}$  and energies in units of the charging energy of an isolated nanoparticle  $E_c^{isl} = 1/(2C^{isl})$ , with  $C^{isl}$  the nanoparticle capacitance when it is isolated. Here and in the following the electronic charge  $e = 1$ . As  $d/r^{isl}$  decreases, the charges in an island feel more the effects of charges in other islands. In this sense we say that decreasing the spacing  $d/r^{isl}$  increases the range of interactions. Experimentally arrays in which the metallic nanoparticles are capped with thiols have  $d/r^{isl} \sim 0.5$ . Arrays self-assembled via other types of molecules, like DNA, allow for the investigation of larger  $d/r^{isl}$  values.

We model each nanoparticle with a continuum level spectrum. The tunneling barriers which separate them have a resistance much larger than the quantum of resistance and we treat the transport at the sequential tunneling level<sup>23</sup>. To analyze the transport the array is sandwiched between two large electrodes. We assume that the electrodes are not ideal voltage sources, but have finite self-capacitances. The potential on the leads will thus fluctuate in response to all tunneling events, even those that do not directly involve the electrodes. For a more extensive discussion of these assumptions see<sup>56</sup>

The energy of the system is given by

$$F = \frac{1}{2} \sum_{\alpha,\beta=0}^{N+1} Q_\alpha C_{\alpha\beta}^{-1} Q_\beta + \sum_{i=1}^N Q_i \phi_i^{dis}. \quad (1)$$

Labels 0 and  $N + 1$  refer to source and drain electrodes and  $1, \dots, N$  to the islands. Latin capital and lower case letters are used to denote electrodes and islands respectively. Greek indexes will be used when the labels refer to both islands and electrodes.  $\phi_i^{dis}$  is a random potential at each island, present in charge disordered arrays, and zero in the clean case. Charges  $Q_0$  and  $Q_{N+1}$  maintain source and drain electrodes at potentials  $V_0$  and  $V_{N+1}$ , respectively.

The electrostatic interactions in our system are defined through an inverse capacitance matrix  $C^{-1}$  that directly includes all the conductors in our system. All the elements  $C_{\alpha\beta}^{-1}$  are positive. The inverse capacitance matrix is symmetric,  $C_{\alpha\beta}^{-1} = C_{\beta\alpha}^{-1}$ , and has dimension  $(N+2) \times (N+2)$ , i.e. it includes the electrodes. We have developed two numerical methods to calculate the interaction potential (inverse capacitance matrix) of an array of spheres. These methods are explained in Appendix I. The properties of this interaction, how it compares to previous calculations for the case of cubic, cylindrical (with array and island axis collinear) and disk shaped islands (with array and island axis perpendicular) and

the screening effect of the electrodes are discussed in Appendix II. For simplicity we have considered two large spherical leads. The coupling between the islands and the electrodes is included through  $C_{i,K}^{-1}$  and  $C_{K,i}^{-1}$ .

The current is computed numerically by means of a Monte Carlo simulation, described in<sup>33,56</sup>. It is controlled by the probability of a tunneling process, given by

$$\Gamma(\Delta E) = \frac{1}{R} \frac{\Delta E}{\exp(\Delta E/K_B T) - 1} \quad (2)$$

Here  $R$  is the resistance of the junction through which tunneling takes place and  $\Delta E$  is the difference between the energy of the system before and after the tunneling event. In the following we restrict the discussion to zero temperature. Then  $\Gamma(\Delta E) = -\Delta E/R_T \Theta(-\Delta E)$ . It is finite only when  $\Delta E$  is negative.

After a bit of algebra, the change in energy due to a tunneling event from  $\alpha$  to  $\beta$  can be rewritten as

$$\Delta E = E_{\alpha,\beta}^{e-h} + (\phi_\beta - \phi_\alpha). \quad (3)$$

Here, the excitonic energy  $E_{\alpha,\beta}^{e-h}$  necessary to create an electron-hole pair in an uncharged array is given by

$$E_{\alpha,\beta}^{e-h} = \frac{1}{2} C_{\alpha\alpha}^{-1} + \frac{1}{2} C_{\beta\beta}^{-1} - C_{\alpha\beta}^{-1}. \quad (4)$$

The second term in (3) can be seen as the potential difference between the sites involved in the tunneling. At the electrodes  $\phi_0 = V_0 = \alpha V$  and  $\phi_{N+1} = V_{N+1} = (\alpha - 1)V$ , where  $V$  is the bias potential and we have introduced the bias asymmetry parameter  $\alpha$  as in ref.<sup>56</sup>. Both  $\alpha = 1/2$ , also denoted as symmetric bias, and  $\alpha = 1$  have been used in the literature.  $\alpha$  characterizes how the bias voltage is partitioned between source and drain chemical potential shifts. Since no physical properties depend on the overall zero of energy, varying  $\alpha$  in our model is entirely equivalent to rigidly shifting all impurity potentials by  $-\alpha V$ . Since in our model all transport occurs by transfer between adjacent nanoparticles, the evolution of a nanoparticle array as the bias voltage is applied is sensitive to  $\alpha$ , and we believe that the dependence on  $\alpha$  could in principle be observable, see discussion in<sup>56</sup>.

At the islands the potential can be decomposed into three terms  $\phi_i = \phi_i^{dis} + \phi_i^{pol} + \phi_i^{ch}$ , the disorder potential  $\phi_i^{dis}$  due to random charges in the substrate, the polarization potential  $\phi_i^{pol}$  at the island induced by the electrodes at finite bias and the potential due to the charges in the nanoparticles  $\phi_i^{ch}$ . Here

$$\phi_i^{pol} = \lambda_i^\alpha V \quad (5)$$

with

$$\lambda_i^\alpha = C_{gen}^2 \left[ \alpha \left( C_{i0}^{-1} C_{N+1,N+1}^{-1} - C_{i,N+1}^{-1} C_{N+1,0}^{-1} \right) + (\alpha - 1) \left( C_{iN+1}^{-1} C_{00}^{-1} - C_{i0}^{-1} C_{N+1,0}^{-1} \right) \right]. \quad (6)$$

and

$$C_{gen}^2 = \frac{1}{C_{00}^{-1}C_{N+1,N+1}^{-1} - (C_{N+1,0}^{-1})^2}. \quad (7)$$

The charging potential

$$\phi_i^{ch} = \sum_{j=1}^N Q_j \tilde{C}_{ij}^{-1} \quad (8)$$

with

$$\tilde{C}_{ij}^{-1} = C_{ij}^{-1} + C_{gen}^2 \left[ C_{0,N+1}^{-1} \left( C_{iN+1}^{-1} C_{j0}^{-1} + C_{i0}^{-1} C_{j,N+1}^{-1} \right) - C_{00}^{-1} C_{N+1,i}^{-1} C_{j,N+1}^{-1} - C_{N+1,N+1}^{-1} C_{i0}^{-1} C_{j0}^{-1} \right]. \quad (9)$$

$\tilde{C}^{-1}$  can be interpreted as a modification of the interaction between the charges in the islands due to the proximity of the electrodes at a fixed potential. For the case  $i = j$  in which both charges are on the same island this modification was already discussed in<sup>33</sup>, as the interaction of a soliton with a passive edge. Expression (9) shows that not only when the charges are in the same island, but also when they occupy different islands, their effective interactions are modified by the presence of the voltage-biased leads. Two types of terms can be differentiated in the modification of this interaction. The last two terms in (9) or direct terms, can be viewed as the interaction between a charge in island  $i$  and the image charge at one of the electrodes induced by the charge in island  $j$ . This term is affected by the presence of the other electrode. On the other hand, the terms containing  $C_{0N+1}^{-1}$ , or indirect terms, reflect the interaction between the image charges in both electrodes. Direct and indirect terms have opposite sign. The direct term reduces the effective interaction; the indirect one increases it. We emphasize that (3) to (9) follow from (1) after straightforward and trivial algebra. We have just defined a few quantities and split the change in energy  $\Delta E$  and potential  $\phi_\alpha$  in several terms to facilitate the physical interpretation of the transport properties.

We can also define the potential drop at each junction

$$\Phi_i = \phi_i - \phi_{i-1} \quad (10)$$

with the corresponding disorder, polarization and charging terms  $\Phi^{dis}$ ,  $\Phi^{pol}$ , and  $\Phi^{ch}$ . Label  $i$  for a junction runs from 1 to  $N + 1$  and refers to the one between conductors  $i - 1$  and  $i$ . The polarization potential drop at each junction,

$$\Phi_i^{pol} = \Lambda_i^\alpha V = (\lambda_i^\alpha - \lambda_{i-1}^\alpha) V, \quad (11)$$

does not depend on the resistance of the junctions, but on the electrostatic interactions of each island with the voltage-biased leads. Here  $\lambda_0^\alpha = \alpha$  and  $\lambda_{N+1}^\alpha = \alpha - 1$ .

A linear drop of the polarization potential implies  $\phi_i^{pol} = \left( \alpha - \frac{i}{N+1} \right) V$ , requires  $\Lambda_i^\alpha = 1/(N + 1)$  for all

junctions and independence on  $\alpha$ . From (6) we see that a priori  $\lambda_i^\alpha$  depends both on the geometry of the electrodes and the array and on how this is biased. It depends on how the charges in the islands and the electrodes interact. For most capacitance matrices, in particular for the capacitance matrices discussed here, the polarization potential is not linear in the island label  $i$  and the potential drops are larger close to the biasing leads. In the on-site case, discussed in ref.<sup>56</sup>  $\Lambda_i^{\alpha\{onsite\}}$  is finite only at junctions 1 and  $N + 1$  and given by  $\Lambda_1^{\alpha\{onsite\}} = \alpha$  and  $\Lambda_{N+1}^{\alpha\{onsite\}} = \alpha - 1$ . In general, as the range of the interactions between charges increases,  $\Lambda_i^\alpha$  is more homogeneous

In previous models<sup>34</sup>  $C^{-1}$  had dimension  $N \times N$  and the inverse self-capacitances of the electrodes,  $C_{00}^{-1}$  and  $C_{N+1,N+1}^{-1}$ , and the inverse mutual capacitances between them,  $C_{0,N+1}^{-1} = C_{N+1,0}^{-1}$ , were neglected. In our model  $C_{K,L}^{-1}$  are small quantities whose values will not significantly affect the quantitative results. These other models do not include the indirect term in (9) either. On the other hand, an expression analogous to (5) can be defined in other models. For example, in the model previously discussed by Middleton and Wingreen<sup>34</sup>, with an  $N \times N$  capacitance matrix, the interaction between an island and an electrode is given by the interaction of the charge of the island with charges induced by the electrode in the islands immediately adjacent to the electrode. This interaction results in a polarization potential characterized by

$$\lambda_i^{MW,\alpha} = C_{i-el} (\alpha C_{1i}^{-1} - (\alpha - 1) C_{Ni}^{-1}) \quad (12)$$

Here  $C_{i-el}$  is the capacitance between the source or drain electrode and an adjacent island. In this model, except in the extreme long-range case, see below, the polarization potential does not decay linearly with distance and depends on the asymmetry of the bias potential. Other models, however, impose a uniform polarization drop through the array<sup>59</sup>

As discussed in<sup>56</sup> and section VI, even if the polarization potential does not drop linearly and is independent on the junction resistance, the average total potential drop depends on the resistance (via the average charge occupation of the islands) and for homogeneous resistances a linear drop is partially recovered at large bias voltages.

Whenever not specified we assume that all the junction resistances  $R_i$  are equal and given by  $R_T$ . The effect of non homogeneous resistances will be studied in two ways. In the first case, one of the junction resistances at a given position is larger than the other ones (given by  $R_T$ ). In the second case the value of the resistances, varying in between two values is randomly assigned to the junctions. To mimic that disorder in resistances originates in variations in distances between the islands and the exponential dependence of the junction resistance in the distance between islands the junction resistance is given by  $R = R_0 \exp(\gamma dist)$  with  $R_0$  and  $\gamma$  input parameters and  $dist = 1 + random/2$ . Here  $random$  is a

random number between 0 and 1. In the paper, we have used  $R_0 = 1.1825R_T$  and  $\gamma = 1.526, 1.95, 2.84$ . With these values the resistance changes respectively between  $(5-11)R_T$ ,  $(8-21)R_T$  and  $(23-83)R_T$ .

### III. SCREENING OF DISORDER POTENTIAL

Charged impurities trapped in the substrate underlying the nanoparticle array create random potentials at the nanoparticles. In molecularly assembled arrays, charge transfer to the organic molecules surrounding the nanoparticles results in non-integer random charges at the islands<sup>60</sup>. Charging disorder is included in our model through a random potential at each island  $\phi_i^{dis}$ . In principle,  $\phi_i^{dis}$  take values larger than the charging energy  $E_c^{isl}$ . However, for large values of the disorder potential, charges flow to compensate for these large fluctuations. In this section we analyze the effect of the long-range interaction on the final distribution of disorder potential as compared to the case with onsite interactions. We find that the distribution of probabilities  $P(\phi_i^{dis})$  and  $P(\Phi_i^{dis})$  are modified. The maximum and minimum values of  $\{\phi_i^{dis}\}$  and  $\{\Phi_i^{dis}\}$  are modified compared to the short range case and given by  $\pm C_{ii}^{-1}/2$  and  $E_i^{e-h}$ . Correlations between the disorder potentials of neighboring islands are introduced.

If interactions between the charges are short-range, ( $C_{ij}^{-1} = \delta_{ij}$ ), the set of disorder potentials  $\{\phi_i^{dis}\}$ , once the screening of the potential due to the mobile charges is taken into account, is uniformly distributed in the interval  $-E_c^{isl} \leq \phi_i^{dis} \leq E_c^{isl}$ . The probability associated with each pair,  $(\phi_i^{dis}, \phi_{i-1}^{dis})$ , is a constant, see Fig. 1 and the distribution of the probabilities of the potential drops due to disorder across the array junctions,  $\Phi_i^{dis} = \phi_i^{dis} - \phi_{i-1}^{dis}$ , has the form<sup>48</sup>

$$P(\Phi^{dis}) = \frac{1}{\Phi_{MAX}^{dis}} \left( 1 - \frac{|\Phi^{dis}|}{\Phi_{MAX}^{dis}} \right) \quad (13)$$

and  $\Phi_{MAX}^{dis} = 2E_c^{isl}$ . In the presence of long-range interactions, the charges which flow to compensate the large fluctuations of the disorder potential, influence the value of the total potential at neighboring islands. As a consequence, the screened disorder is correlated<sup>48</sup>. The probability of each pair  $(\phi_i^{dis}, \phi_{i-1}^{dis})$  is no longer a constant.  $P(\Phi^{dis})$  depends on the inverse capacitance matrix  $C^{-1}$ . In order to analyze these correlations and obtain the proper disorder potential distribution we assign the potentials by first randomly assigning potentials to the islands  $\phi_i^{dis-bare}$ , in the interval  $-W \leq \phi_i^{dis-bare} \leq W$  with  $W$  larger than the charging energy. We then find the equilibrium configuration of charges  $\{Q_j^{sc}\}$  that occupy the array with island disorder potentials  $\{\phi_i^{dis-bare}\}$  and grounded leads ( $V_0 = V_{N+1} = 0$ ) and redefine the

potentials at each site using the expression

$$\phi_i^{dis} = \sum_{j=1}^N \tilde{C}_{ij}^{-1} Q_j^{sc} + \phi_i^{dis-bare}. \quad (14)$$

The effect of the screening charges  $\{Q_j^{sc}\}$  is included in the redefined potentials  $\{\phi_i^{dis}\}$  so we then reset the number of charges at each site to zero to avoid doublecounting the charge when we calculate the total electrostatic energy of our system.

Following the redefinition of the disorder potentials, we find that on average the distribution of the disorder potentials  $\{\phi_i^{dis}\}$  and the disorder potential drops  $\{\Phi_i^{dis}\}$  between adjacent islands are independent of  $W$ . The values of  $\{\phi_i^{dis}\}$  and  $\{\Phi_i^{dis}\}$  are bound by  $\pm C_{ii}^{-1}/2$  and  $\pm E_i^{e-h}$  respectively, as the total energy of the system is at a global minimum when the original disorder configuration  $\{\phi_i^{dis-bare}\}$  is screened out by the charges  $\{Q_j^{sc}\}$ . When in this state, adding an additional charge to any island in the array increases the energy of the system. The energy of adding an additional charge to an island from a large electrode outside the system with negligible self inverse capacitance is given by  $E_i^{add} = (1/2)C_{ii}^{-1} \pm \phi_i^{dis}$  where the top (bottom) sign refers to the change in energy of the system as a result of adding a positive (negative) charge to island  $i$ . Since  $E_i^{add} > 0$  when the array is in equilibrium, the disorder potential values must lie between  $\pm(1/2)C_{ii}^{-1}$ . The magnitude of this quantity equals  $E_c^{isl}$  in the onsite limit and decreases as the strength and range of the Coulomb interactions increases, see Appendix II. Additionally when the array is in equilibrium state, the energy to hop between all pairs of adjacent sites must be greater than zero. From (3), the disorder potential differences  $\Phi_i^{dis}$  are restricted between  $\pm E_i^{e-h}$ .  $E_i^{e-h}$  equals  $2E_c^{isl}$  in the onsite limit and decreases with decreasing  $d/r^{isl}$ , as shown in Fig. 8.

Fig. 1(a) and (b) compare  $P(\phi_i^{dis})$  and  $P(\Phi_i^{dis})$  for arrays with purely onsite interactions ( $C_{i \neq j}^{-1} = 0$ ) with arrays with long range interactions ( $C_{i \neq j}^{-1} \neq 0$ ) at two spacings,  $d/r^{isl} = 0.5$  and  $d/r^{isl} = 10$ . In all cases,  $\phi_i^{dis}$  and  $\Phi_i^{dis}$  are calculated for arrays with 50 islands in between two grounded leads. The histograms average the values of the potentials of all islands and the values of the potential drops between all adjacent islands over many realizations of disorder ( $O(> 10^4)$ ). The smaller spacing,  $d/r^{isl} = 0.5$ , is typical of chemically assembled nanoparticle arrays. The larger spacing,  $d/r^{isl} = 10$ , is atypical of arrays in most experiments but is mainly included as a pedagogical example because it has interactions among islands that are finite yet comparable to the onsite case that is often used to describe experiments<sup>3,34,48</sup>. Arrays recently synthesized<sup>7</sup> have large  $d/r^{isl}$  values. In Fig. 1(a),  $P(\phi_i^{dis})$  is a constant between  $\pm E_c^{isl}$  for the onsite case. As the range of interactions increases (decreasing  $d/r^{isl}$ ), the width of  $P(\phi_i^{dis})$  decreases because the disorder potential values are bound by  $\pm 0.5C_{ii}^{-1}$ . Increasing Coulomb interactions also increases (decreases) the

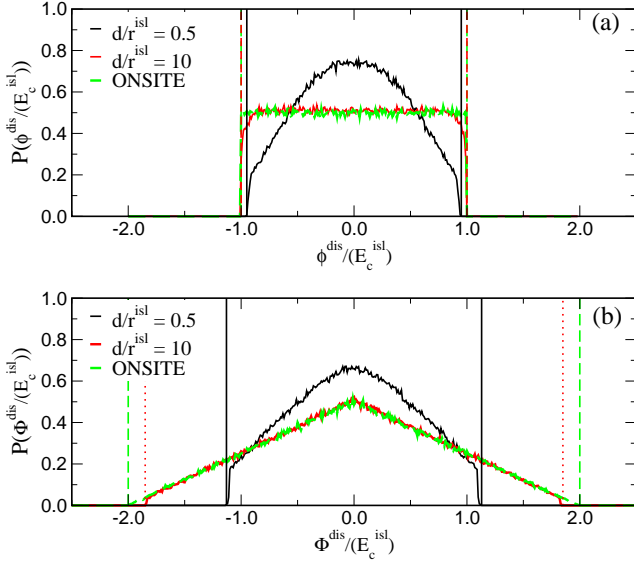


FIG. 1: Probability distributions of disorder potentials  $\phi^{dis}$  in (a), and disorder potential differences  $\Phi^{dis}$  in (b), due to disorder for 50-island arrays with purely onsite interactions and with long range interactions at two spacings:  $d/r^{isl} = 0.5$  and 10. The onsite  $\Phi^{dis}$  distribution is described by Eq.(13) with  $\Delta\phi_{MAX}^{dis} = E_{i,i-1}^{e-h, onsite} = 2E_c^{isl}$  where  $E_c^{isl} = 1/(2C_{ii}^{isl})$ . For all the cases,  $P(\phi^{dis})$  ( $P(\Phi^{dis})$ ) is finite valued for  $\phi^{dis}$  ( $\Phi^{dis}$ ) between  $\pm 0.5C_{ii}^{-1}$  ( $\pm E_i^{e-h}$ ) which decreases with decreasing spacing. As the spacing decreases, the probability of having  $\Phi^{dis}$  and  $\phi^{dis}$  values close to zero increases. Vertical lines are included as guidelines to emphasize the edges of the distributions.

probability of small (large) values of  $|\phi_i^{dis}|$ . In Fig. 1(b), the onsite  $P(\Phi_i^{dis})$  distribution is given by (13). Similar to the trends in Fig. 1(a), as the range of Coulomb interactions increases, the width of the distribution decreases and the probability of small (large)  $|\Phi_i^{dis}|$  values increases (decreases). The increased probabilities of small  $|\Phi_i^{dis}|$  are due to Coulomb correlations that make it more likely for the disorder potentials of neighboring islands to have similar values. See Fig. 2. Increasing the range of Coulomb interactions leads to a greater relative reduction in the width of  $P(\Phi_i^{dis})$  than  $P(\phi_i^{dis})$  because the former are bound by  $\pm E_i^{e-h}$  whereas the latter are bound by  $\pm 0.5C_{ii}^{-1}$ . In the onsite case,  $E_i^{e-h}$  equals  $2E_c^{isl}$  for all junctions between two islands and increasing Coulomb interactions can reduce  $E_i^{e-h}$  significantly due to an decrease (increase) in  $C_{ii}^{-1}$  ( $C_{i,i\pm 1}^{-1}$ ). See (4).

Our results for  $P(\Phi_i^{dis})$  differ to some extent from those by Elteto et al<sup>48</sup>, calculated with an inverse capacitance matrix  $C_{ij}^{-1}$  that is finite only for nearest neighbors and charge disorder modelled by a set of stationary quenched charges. Elteto et al<sup>48</sup> distributions are bound by  $\pm C_{ii}^{-1}$  instead of by  $E_i^{e-h}$  due to the lack of correlations in their quenched disorder model. We permit the interactions among the screening charges to determine whether or not the disorder potentials are correlated.

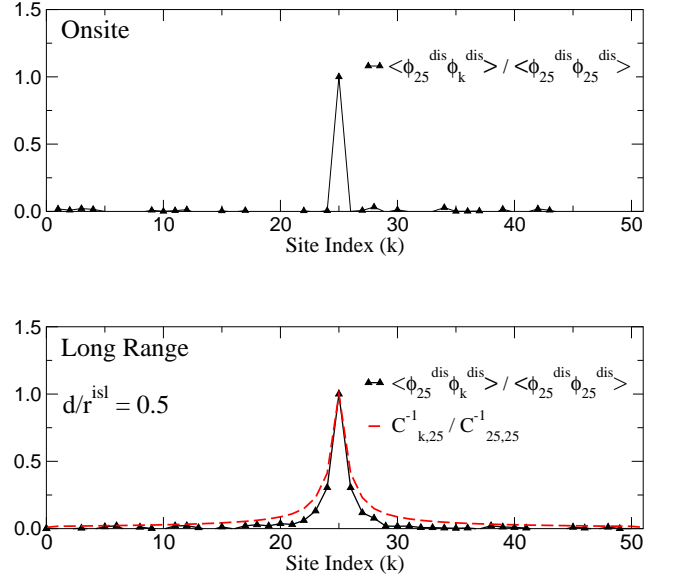


FIG. 2: Comparison of  $\langle \phi_{25}^{dis} \phi_k^{dis} \rangle$  normalized by  $|\phi_{25}^{dis}|^2$  for 50-island arrays with onsite (top plot) versus long range (bottom plot) Coulomb interactions. In the presence of long-range interactions between the charges, the values of the disordered potentials are also correlated.  $C_{k,25}^{-1}$  normalized by  $C_{25,25}^{-1}$  is included in the long range case to show that correlations in the disorder potentials are related to, but decay faster than the  $C^{-1}$  elements.

In Fig. 2, we plot  $\langle \phi_i^{dis} \phi_k^{dis} \rangle$  to show how interactions among charges affect the correlations among disorder potentials. In the onsite case, correlations are finite only if  $i = j$ . In this case, the disorder potentials of different islands are uncorrelated. In the case of long-range interactions with  $d/r^{isl} = 0.5$ , correlations are maximal when  $i = j$ , but they do not vanish for  $i \neq j$ .  $\langle \phi_i^{dis} \phi_k^{dis} \rangle$  is finite for at least  $|i - k| \leq 3 - 4$ . The correlation of disorder decays faster than the interactions as shown in the figure. The correlations between  $\phi_i^{dis}$  and its nearest neighbors  $\phi_{i\pm 1}^{dis}$  make it more likely for the disorder potential differences  $\Phi_i^{dis}$  to have small magnitudes.

#### IV. THRESHOLD

The threshold voltage is the minimum voltage which allows the flow of current. In this section we analyze the threshold voltage of one-dimensional arrays with long-range interactions for both clean and disordered systems. As in the short-range case the threshold is completely determined by energetic considerations and is independent of junction resistance disorder. In the clean case we find that the threshold equals the minimum voltage necessary to create an electron-hole pair and increases with the number of particles at a rate which depends on  $d/r^{isl}$ . For charge disordered arrays the average threshold is reduced compared to the onsite interactions case,

and increases linearly with the number of islands, with a slope that decreases with decreasing  $d/r^{isl}$ , i.e. with increasing the range of the interaction.

When the interaction strength between charges at the nanoparticle and those at the electrodes does not vanish for any particle the polarization potential drop at every junction is finite. In a clean array, the potential gradient created by this polarization potential drop allows current once an electron-hole pair is created, opposite to what happens in the onsite case. As a result, the threshold voltage equals the minimum voltage which allows the creation of an electron-hole pair.

The cost in energy to create an electron-hole pair in junction  $i$  in an uncharged array (i.e. an array in which the nanoparticles have no excess charges) is  $\Delta E = E_i^{e-h} - \Lambda_i^\alpha V$ . We can define a junction dependent threshold voltage for creating an electron-hole pair  $V_i^{TH,\alpha} = E_i^{e-h}/\Lambda_i^\alpha$ . In the onsite limit  $V_i^{TH,\alpha}$  is finite only at one or both contact junctions and infinite at the bulk, but with long-range interactions  $V_i^{TH,\alpha}$  is finite at every junction. For those cases analyzed, we have found that due to the smaller value of the excitonic energy and the larger potential drop  $V_i^{TH}$  is smallest at the contact junctions and the threshold voltage is controlled by them.

Figs. 3(a) and (b) show the dependence of the threshold voltage  $V_T$  of clean, symmetrically biased arrays with long-range interactions on the number of islands in the array  $N$  and on the spacing between array sites,  $d/r^{isl}$ . The threshold voltage is determined by those factors that define the polarization potential drops across the contacts,  $\Lambda_1^\alpha$  and  $\Lambda_{N+1}^\alpha$ .  $V_T$  increases with increasing  $N$  because the fraction of the polarization potential which drops across the contact junctions decreases as  $N$  increases. As the spacing between the leads increases, the polarization potential drop across each contact decreases until eventually it reaches a minimum value at which the polarization of each contact is only due to the interaction of each contact with the lead closest to it. As a result,  $V_T$  increases sublinearly with increasing  $N$  and eventually saturates. For  $N$  and  $d/r^{isl}$  large enough that the polarization potential drop across the contacts is not strongly influenced by interactions with the opposite lead, decreasing the array spacing decreases the polarization potential drop across the contact junctions and the threshold increases. For  $N$  and  $d/r^{isl}$  small enough that both leads strongly influence the polarization of both contact junctions, decreasing the spacing increases the polarization potential drop across the leads and the threshold decreases. The potential drops and threshold can be estimated by using an unscreened  $r^{-1}$  model for the inverse capacitance elements associated with the leads,  $C_{i,0}^{-1}$  and  $C_{i,N+1}^{-1}$ . These estimates are included as dashed lines in Figs. 3(a) and (b).

As shown in the inset of Fig. 3(b)  $V_T$  changes smoothly with  $\alpha$ , contrary to the peak-valley structure found in the onsite interaction case<sup>56</sup>. The threshold voltage depends less on  $\alpha$  as  $N$  increases and as  $d/r^{isl}$  decreases because

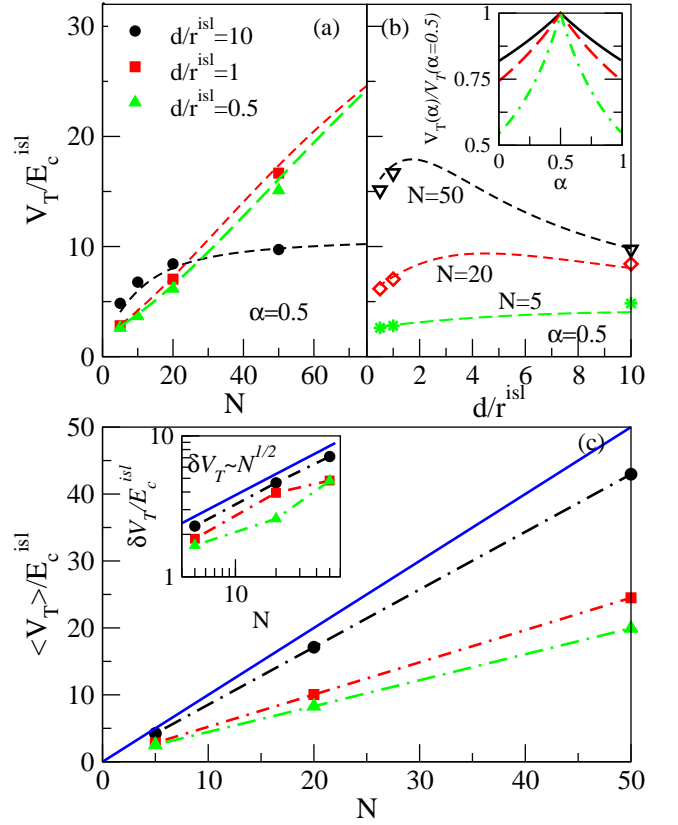


FIG. 3: (a) and main figure in (b): With symbols it is respectively plotted the threshold voltage  $V_T$  of symmetrically biased arrays  $\alpha = 0.5$ , with no disorder as a function of number of islands  $N$  and of array spacing  $d/r^{isl}$  for the inverse capacitances calculated as described in appendix I. As described in the text, the threshold voltage of clean arrays is controlled by the value  $\Lambda_i^\alpha$  at the contact junctions. The dashed lines are estimates of the threshold voltage that use a  $r^{-1}$  interaction to approximate the polarization potential drops across the contact junctions  $\Lambda_1^\alpha$  and  $\Lambda_{N+1}^\alpha$ . Inset in (b): Threshold voltage of clean arrays for several array parameters as a function of  $\alpha$  normalized to the value for a symmetrically biased array. From top to bottom  $d/r^{isl} = 0.5, N = 50$ ;  $d/r^{isl} = 0.5, N = 20$ ; and  $d/r^{isl} = 10, N = 50$ . (c) Main figure: Average threshold voltage of disordered arrays versus the array length at three different array spacings. The solid line shows the dependence of the average threshold on array length in the limit of onsite interactions. The inset shows the root mean square deviation of the threshold voltage distribution. For small  $d/r^{isl}$  it deviates from the  $N^{1/2}$  dependence found in the onsite case (in solid line). In inset and main figure dashed-dot lines are a guide to the eye and same legend as in (a) applies

the applied voltage drops more homogeneously across the array junctions. This dependence disappears completely if the polarization potential drops linearly. In this last case the threshold voltage of clean arrays would be  $V_T = (N + 1)E_c^{isl}$ . This threshold is linear in the number of particles, as in the onsite case, but its origin of linearity and its slope differs in both cases.

In the charge disordered onsite case every up-step in the disorder potential prevents current flow and has to be compensated by a charge gradient. As a result, the threshold voltage is controlled by the number of up-steps, but this is not the case for long-range interactions. In the long-range case the situation is more complex. Due to the finite polarization potential drop at the inner junctions the number of junctions which prevent the flow of current is reduced, compared to the onsite case. Up-steps in the disorder potential drop can localize the charge only if its value is larger than the polarization potential drop at the same junction. In some cases in which there is finite polarization drop at a junction, that is slightly smaller than the energy cost for tunneling it is possible that a small increase in the voltage in the electrodes permits the tunneling. Increasing the voltage above the minimum bias voltage which permits the generation of electron-hole pairs will, in some cases, but not always, result in a negative potential drop at the given junction allowing the flow of charges. But, quite often, the entrance of more charges and the creation of a charging potential gradient will be required in a similar way as it happened in the onsite case. Note that due to the polarization voltage drop at the bulk, the threshold junction can be other than the contact ones. Moreover, the interaction between charges in different islands decreases the energy for the entrance of a charges with opposite sign and increases the one for the entrance of charges with the same sign. This effect was attributed to an attraction (repulsion) between the injected soliton and an antisoliton (soliton) on the array by Likharev and coauthors<sup>33</sup>. Accumulation of charges in the array increases the threshold voltage. On the other hand a value of  $\phi_i^{dis}$  at the contact islands favourable for the entrance of charge unto the array can decrease it, as the polarization potential drop to allow entrance of charge is smaller. Both mechanisms compete to determine  $V_T$ . For large  $d/r^{isl}$  the accumulation of charges is more important as the voltage drop at the bulk junctions is small and on average  $V_T$  of large arrays will increase compared to the clean array threshold voltage. On the contrary the second effect can be more important for small  $d/r^{isl}$ .

Numerically we have found a linear dependence of the threshold voltage on the number of particles in the array, see Fig. 3(c). Decreasing the array spacing decreases the average thresholds below the threshold values of the arrays in the onsite limit. The expected behavior of the average threshold value as compared to the clean limit, discussed above, is found. Only at the largest array spacing ( $d/r^{isl} = 10$ ) studied do we recover the dependence of the fluctuations of the threshold voltage on array length predicted by Middleton and Wingreen<sup>34</sup>, see inset of Fig. 3(c).

## V. FLOW OF CURRENT

In this section we discuss the three main voltage regimes which can be distinguished in the I-V curve. At voltages very close to the threshold, we show that the current is linear in  $(V - V_T)$ . Contrary to the short-range interaction case, the slope of this linearity depends, not only on the junction resistance and on  $\alpha$ , but also on the number of islands and on  $d/r^{isl}$ . For given  $\alpha$ ,  $N$ ,  $d/r^{isl}$  and  $\{R_i\}$ , in the presence of charge disorder, the slope of the I-V curve close to threshold can depend on the potential disorder configuration. At intermediate voltages steps in the current are smoothed compared to the onsite interaction case. A linear I-V with an offset voltage, closely related to the one found for short range interactions, characterizes the high voltage regime.

### A. Voltages close to threshold

For the onsite interaction case we recently resolved the controversy<sup>34,39,54,59</sup> on the power law dependence of current on  $(V - V_T)$ , showing that very close to threshold it is linear<sup>56</sup>. Such a linearity is due to the bottle-neck character of one of the junctions and the linear dependence of the energy for tunneling on the bias voltage. These two assumptions remain valid for long-range interactions, so the linear  $(V - V_T)$  dependence is also found in this case. In the case of clean arrays, the threshold and low-voltage bottle-neck for current are found at the contact junctions and

$$I \sim \frac{\Lambda_{1,N+1}^\alpha}{R_{1,N+1}}(V - V_T) \quad (15)$$

Except for  $\alpha = 1/2$ , for which  $\Lambda_1^{1/2}/R_1$  and  $\Lambda_{N+1}^{1/2}/R_{N+1}$  have to be added in the expression for the slope. Dependence in  $N$ ,  $d/r^{isl}$  and  $\alpha$  via the dependence of  $\Lambda_{1,N+1}^\alpha$  on these parameters is found as seen in Fig.4 (a) and (b). The value of  $\Lambda_i^\alpha$  which appears in the expression of  $V_T$  is the same that controls the linearity of the IV curves very close to threshold. The behavior of the slope of  $I$  vs  $(V - V_T)$  with  $\alpha$ ,  $N$  and  $d/r^{isl}$  is opposite to the one of  $V_T$ . For  $\alpha$  different from  $1/2$ , increasing  $N$  and decreasing  $d/r^{isl}$  decreases the slope because these changes reduce the fraction of the polarization potential that drops across the contact junctions. Biasing the array in a more assymmetric way (increasing  $|\alpha - 1/2|$ ) changes the slope as the fraction of the polarization potential that drops across the contact junction that serves as a bottle-neck at small voltages is modified. The slope does also depend on the junction resistances, similar to the dependence found for onsite interactions<sup>56</sup>, see Fig. 4(c).

The charge disordered case is to some extent different. The above threshold bottle-neck (and below threshold current-blocking) junction is not necessarily either of the contact junctions, so the slope of the linear dependence can be controlled by  $\Lambda_i^\alpha$  with  $i \neq 1, N + 1$ . The junction



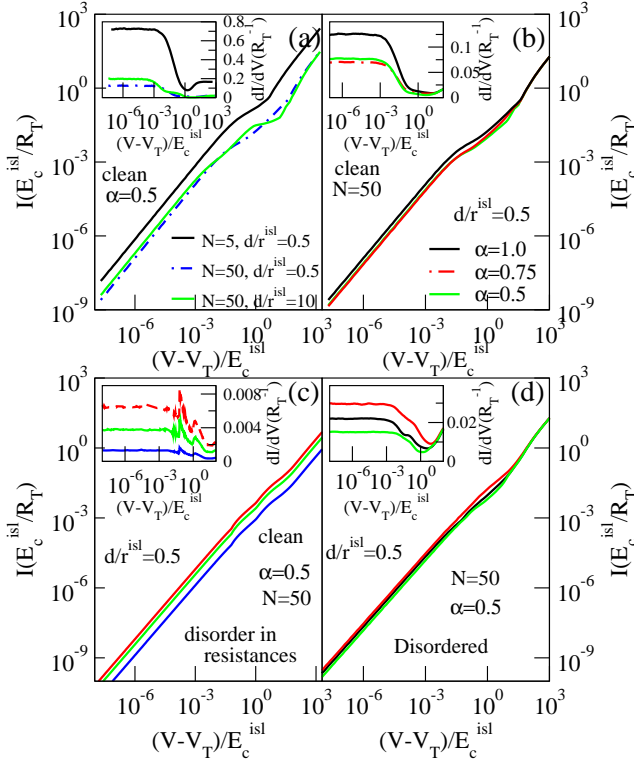


FIG. 4: I-V curves of ordered arrays at voltages very close to threshold. The insets show the derivatives of the I-V curves. Similar to what was found for onsite interactions very close to threshold the I-V is linear. The linear regime ends at voltages  $V - V_T \sim 10^{-2} E_c^{isl}$ , much lower than the values used in experiments to check the power-law dependence close to threshold. (a) shows how varying the length and spacing of symmetrically biased arrays affects the slopes of the linear regimes, due to the change in the polarization potential drop factors  $\Lambda_i^\alpha$  and correspondingly the fraction of potential which drops in the junction which acts as bottle-neck. (b) In a similar way, the slope depends on how symmetrically is the array biased. (c) plots the I-V curves and derivatives corresponding to clean arrays with equal length,  $d/r^{isl}$  and  $\alpha$  but different junction resistances. Resistances in these plots vary randomly in between  $(5 - 11)R_T$ ,  $(8 - 21)R_T$  and  $23 - 83R_T$  in top, middle and lower curves. (d) I-V curves corresponding to three different realizations of charge-disordered arrays with all junction resistances equal  $N = 50$  and  $\alpha = 0.5$ . Contrary to what was found for onsite interactions the slope of the low-voltage linear current can be different for different arrays with the same nominal parameters if there is charge disorder. This reflects that the bottle-neck is not necessarily a contact junction but can be a junction in the bulk.

that acts as the bottle-neck depends on the particular disorder configuration. This is shown in Fig. 4(d), which plots the current and its derivative with respect to voltage for several configurations of disorder corresponding to the same value of  $d/r^{isl}$ ,  $N$  and  $\alpha$  and the same junction resistances. A similar dependence of the slope on the charge disorder configuration was not present in the short-range case, as the energy gain for tunneling is di-

rectly modified by changes in the bias potential only at the contact junctions, at least for  $\alpha = 1/2$ . The slope is generally larger (smaller) when the bottleneck junction lies closer to the edge (middle) of the array. Changing  $\alpha$  also modifies the slope of the disordered case, not shown. This modification can be due to the change of  $\lambda_i^\alpha$  with or without a change in the bottleneck junction.

## B. Intermediate voltage regime

As in the onsite case<sup>56</sup> the linearity of the current disappears when the bottle-neck description stops being valid. This happens at very small values of  $(V - V_T) \sim 10^{-2} E_c^{isl}$ . It is easy to show how this situation leads to sublinear behavior. Assume that the transport happens through a sequence of  $N + 1$  tunneling processes and consider a bottle-neck process with rate  $\Gamma_i = R_i^{-1} \Lambda_i^\alpha \tilde{V}$  with  $\tilde{V} = V - V_T$  and another process in the sequence with rate  $\Gamma_j = R_j^{-1} (E_j^T + \Lambda_j^\alpha \tilde{V})$ . Here  $E_j^T$  is the gain in energy of the second process at  $V = V_T$ . If these two processes have rates much smaller than the rest of processes in the sequence, the current can be approximated by

$$I \sim \frac{1}{\tau_i + \tau_j} = \frac{R_i^{-1} \Lambda_i^\alpha \tilde{V}}{1 + \frac{R_i^{-1} \Lambda_i^\alpha \tilde{V}}{R_j^{-1} (E_j^T + \Lambda_j^\alpha \tilde{V})}} \sim R_i^{-1} \Lambda_i^\alpha \tilde{V} \left( 1 - \frac{R_i^{-1} \Lambda_i^\alpha \tilde{V}}{R_j^{-1} E_j^T} \right) \quad (16)$$

The slope of the current and the lost of linearity depends on the resistance of the junctions, as was also seen in the onsite case<sup>56</sup>. In the clean long-range case comparing the values of  $\Lambda_i^\alpha$  the linear behavior lasts longer in shorter arrays, smaller  $d/r^{isl}$  and smaller  $\alpha$ , as in these cases the values of  $\Lambda_i^\alpha$  are more homogenous throughout the array. The disordered long-range case is more complex. Due to the non-homogeneous increase in polarization voltage drop a junction which has a small energy gain can increase this gain more than other junctions when the applied voltage increases and the dependence of the slope with the array parameters is not so easily predicted.

If the value of the voltage is increased further several tunneling processes are energetically allowed at each step in a sequence and the discussion of transport becomes more complex due to the multiple choices available and the polarization potential drop at the bulk junctions. Above the linear regime there is a region of smoothed steps in the I-V curve. Decreasing  $d/r^{isl}$  smooths the steps and for small  $d/r^{isl}$  they are hardly distinguishable. This behavior is seen in Fig. 5(a) which compares the onset of current, at voltages not extremely close to threshold, for several array parameters. For clarity the curves have been plotted as a function of  $(V - V_T)$ . The staircase profile differs in all these cases. The top curve



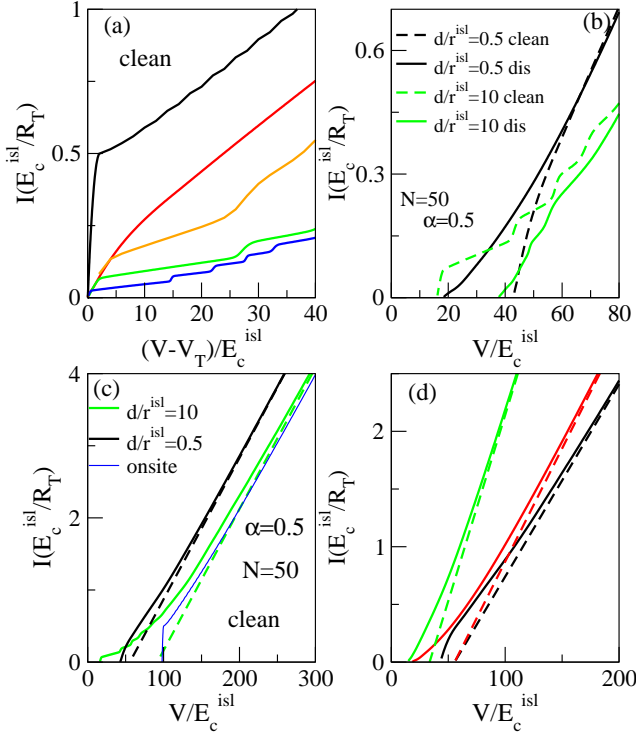


FIG. 5: In (a) and (b) the I-V characteristics show the Coulomb staircase and correspond to clean arrays with homogeneous resistances. (a) shows five curves for different interaction ranges and lengths. From top to bottom, the first four curves correspond to  $\alpha = 0.5$  and respectively to  $N = 50$  with onsite interaction;  $N = 50$  with  $d/r^{isl} = 0.5$ ;  $N = 30$  with  $d/r^{isl} = 10$ ;  $N = 50$  with  $d/r^{isl} = 10$ . The lowest curve corresponds to a  $N = 50$  and  $\alpha = 1$  and  $d/r^{isl} = 10$ . The threshold voltage has been subtracted.  $V_T$  equals 98, 43, 14, 16 and 9.7 respectively. In the onsite case it is necessary to create a charge gradient at every junction to allow current, but once charge can reach the opposite electrode it flows easily and the I-V shows a large jump close to threshold. For  $d/r^{isl} = 10$  a charge gradient is not created and bulk junctions slow the current flow producing the staircase structure. The step width is smaller for forward bias  $\alpha = 1$  than for symmetric bias, but contrary to the behavior found in the Coulomb staircase for onsite interactions, with long-range interactions the step width is not fixed. The steps are washed out for  $d/r^{isl} = 0.5$  due to a more homogeneous polarization potential drop through the array. (b) I-V curves for disordered arrays with  $d/r^{isl} = 0.5, 10$ . The clean case is included for comparison. (c) I-V in a large voltage scale for clean arrays with homogeneous resistances, from top to bottom solid lines correspond to  $d/r^{isl} = 0.5$ ,  $d/r^{isl} = 10$  and onsite interactions. The dashed lines give the asymptotic predictions for  $d/r^{isl} = 0.5$  and 10. At high voltages all the curves have the same slope given by  $R_{sum}^{-1}$ . The offset voltages differ as the excitonic energies do. In spite of the very different threshold voltage and the different dependence on voltage close to threshold, the  $d/r^{isl} = 10$  I-V curve differs little from the onsite one at high voltages. (d) I-V curves in a large voltage scale corresponding to  $d/r^{isl} = 0.5$  symmetrically biased arrays. From top to bottom  $N = 30$  and  $N = 50$  disordered arrays with homogeneous resistances and a  $N = 50$  clean array with the first resistance ten times larger than the other ones. Dashed lines give the asymptotic predictions. The slope of both  $N = 50$  curves differ, but their offset voltages are the same.

corresponds to an  $N = 50$  array with short-range interactions, previously studied<sup>56</sup>. In this case to allow current flow a charge gradient at each bulk junction has to be created, but once charge can enter the array it flows easily through it. This is reflected in the sharp onset of the current close to threshold. The steps at higher voltages are just barely visible at this scale. Once the polarization voltage at each junction is finite it is not necessary to create a charge gradient at the inner junctions and the steps' shape is modified. The three bottom curves correspond to  $d/r^{isl} = 10$ . Several features can be appreciated in these curves. The step shape is clearly seen. As the potential drop at the inner junction is small, bulk junctions control the flow of currents at each plateau and their slope is small. The slope is larger for shorter arrays, and the step width depends on the value of  $\alpha$ . The dependence of the step width on  $\alpha$  was also found for onsite interactions, but contrary to the short range case, for finite  $d/r^{isl}$  the step width is not a constant throughout the curve as the presence of charges in the array influences the energy cost to add charges from the electrodes, to the first or last island. As also seen in this figure, for small  $d/r^{isl}$  the polarization potential drop at the inner junction is larger and similar to what happened in the onsite case (but for reasons to some extent different) once the charge enters the array it can flow easily. In (b) we can see the different I-V curves in clean and disordered arrays. Specially interesting is the disordered  $d/r^{isl} = 0.5$  I-V characteristic. It looks superlinear, similar to what would be found if a power-law larger than unity is present at these voltages. We have observed that this approximate superlinear type dependence is common in disordered arrays with small  $d/r^{isl}$ . If experimentally the power-law behavior expected close to threshold is measured at these voltages (larger than those at which the linear behavior is predicted) the exponent of the power-law could be erroneously assigned a value larger than one.

### C. Linear behavior at high voltages

At very high voltages, in the onsite interaction case we showed<sup>56</sup> that the current can be approximated by the asymptotic expression

$$I_{asympt} \sim \frac{1}{R_{sum}} \left( V - \sum_{i=1}^{N+1} E_i^{e-h} \right) \quad (17)$$

with  $R_{sum} = \sum_{i=1}^{N+1} R_i$ . The arguments, based on a uniform tunneling rate through all the junctions in this voltage regime, which led to this expression remain valid in the long-range case, with the only change of the quantitative value of the excitonic energies  $E_i^{e-h}$ . The slope of the current does not depend on the range of the interaction or the presence of charge disorder but the offset voltage at which the asymptotic expression cuts the zero current axis, does<sup>56,61,62</sup>. Confirmation of the validity

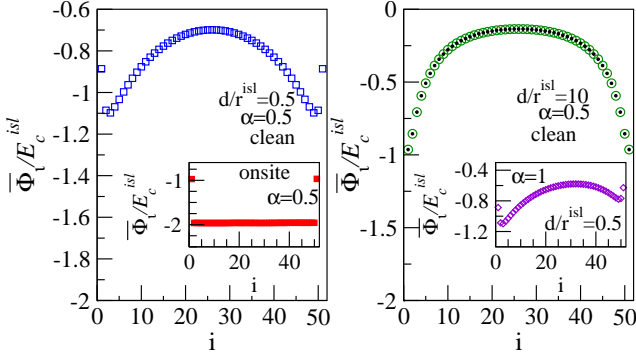


FIG. 6: Average voltage drop close to threshold for  $N = 50$  arrays with different parameters. Both (a) and (b) correspond to clean arrays. Main figures are for  $\alpha = 0.5$  and long-range interaction. The average potential drop essentially equals the polarization potential for each value of  $d/r^{isl}$ , which is plotted as filled small dots in (b) for comparison. This behavior contrasts with the potential due to the charge gradient which has to be created in the onsite case, shown in the inset of (a). As shown by comparing main figure in (a) with the inset in (b) a change in the value of  $\alpha$  modifies  $\Lambda_i$  and correspondingly the potential drop through the array.

of (17) is seen in Figs. 5(c) and (d), where numerical results are compared with the asymptotic behavior predicted by (17). In Fig. 5(c) the I-Vs for symmetrically biased arrays with  $N = 50$  nanoparticles and different interaction range are plotted. At high voltages slopes are equal but the offset voltage to which they extrapolate it is not. Note the difference between the value of threshold and the one of the offset. In particular the  $d/r^{isl} = 10$  curve has a smaller threshold and larger offset than the  $d/r^{isl} = 0.5$ . In Fig. 5(d) the influence of the number of junctions and their resistance in the high-voltage current is reported and shown to be in good agreement with the approximate prediction.

## VI. VOLTAGE DROP

In this section we analyze the effect of long-range interactions in the voltage drop through the array. We differentiate the same three regimes as in previous section. Differences found with respect to the onsite case, previously analyzed<sup>56</sup> are mainly due to the polarization potential drop at the bulk junctions, which vanishes in the onsite limit but is finite when interactions between the charges at the islands and those at the electrodes are long-range.

As discussed in section IV, in a clean array,  $V_T$  is given by the minimum bias voltage which allows the creation of an electron-hole pair. Contrary to the onsite case<sup>56</sup> there is no charge accumulation in the array. It is thus expected that very close to  $V_T$  the voltage drop reflects the polarization drop  $\Lambda_i^\alpha V$  at each junction. The potential drop distribution thus depend on the length of

the array  $N$ , the bias asymmetry  $\alpha$  and on the range of the interactions  $d/r^{isl}$ . This dependence is confirmed in Figs. 6(a) and (b) where the potential drop is plotted for different array parameters. The value of  $\Lambda_i^\alpha$  is included for comparison in Fig. 6(b). The voltage drop is very different from the one found to the onsite case (included in the inset of Fig. 6(a)), where in the bulk it is due to charge accumulation at the islands. The dependence on the value of the resistance is extremely weak even once the polarization potential drop is subtracted (not shown) and not observable, except if the difference in the value of resistances is very large. In the disordered case with long-range interaction it is possible that once charge is allowed to enter the array it can flow. Then the average potential drop is approximately the sum of the disorder potential and the polarization potential. In general, when this happens the threshold voltage is smaller than the one in the clean case as the disorder potential reduces the polarization potential drop necessary at at least one of the contact junctions. But for large  $d/r^{isl}$  is more probable that one or more charges remain stacked in the array, similarly to the case of onsite interactions and the charge potential due to these stacked charges has to be added.

At intermediate voltages, in the Coulomb staircase regime, we saw in the onsite case<sup>56</sup> that the voltage drop through the array shows an oscillatory behavior, with the number of maxima increasing from step to step. A similar behavior is found in Fig. 7(a) corresponding to a clean array and  $d/r^{isl} = 10$ . In Fig. 7(b) for all the voltages plotted the number of maxima is two, and their amplitude decreases until at the largest voltage oscillations cannot be discerned. Comparing with Fig. 5 one realizes that the step number has not changed. The I-V curves reaches the high-voltage regime without showing stepwise behavior.

At high voltages, the potential drop is qualitatively similar to the one found in the onsite case<sup>56</sup>. The voltage drops linearly only after subtracting from each junction the excitonic energy. The sum of the excitonic energies results in the offset voltage. The current is equal to  $(V - V_{offset})/R_{sum}$  and the corresponding voltage drop at each junction is

$$\bar{\Phi}_i^{high} = R_i I + E_i^{e-h} \quad (18)$$

which satisfies  $V = \sum_i \bar{\Phi}_i = I \sum_i R_i + \sum_i E_i^{e-h} = I R_{sum} + V_{offset}$ . Eq.(18) is valid for both ordered and disordered arrays. Some examples of this behavior are shown in are shown in Fig. 7. In Fig. 7(c) we can see that as expected, in the absence of resistance disorder, once the excitonic energy is subtracted the potential drops homogeneously through the array even if there is charge disorder, while it is proportional to the resistance value when resistances are not homogeneous, as in Fig. 7(d).

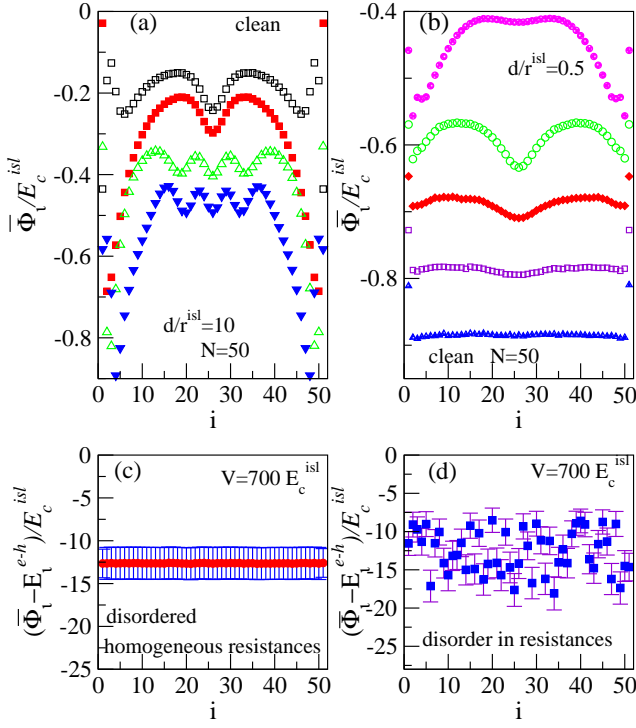


FIG. 7: Average potential drop at the array junctions at intermediate (upper figures) and high voltages (lower figures) for  $\alpha = 0.5$  and  $N = 50$ . Upper figures correspond to clean arrays. Curves in (a) are for  $d/r^{isl} = 10$  and (from top to bottom)  $V = 20, 32, 44, 56 E_c^{isl}$ . The oscillations in average potential found in the onsite case at intermediate bias voltages are still present, and the number of maxima increases in two when going to a higher step. In (b)  $d/r^{isl} = 0.5$  and  $V = 46, 60, 70, 80, 90 E_c^{isl}$ . The number of maxima has not increased in this range of voltages but oscillations are smoothed with increasing bias voltage. In spite of the large value of the voltage the current is still in the first step of the Coulomb staircase, see Fig. 5(a). The potential drop at  $V = 90 E_c^{isl}$  resembles the one at high voltages, homogeneous except by the excitonic term responsible of the offset. In (c) and (d) the excitonic energy has been subtracted from the average potential drop at high voltages. Once this term is subtracted the average potential drop is completely homogeneous through the array in (c) where there is charge disorder, and all resistances are equal but not in (d) which corresponds to a clean array but with resistances which vary randomly between  $(5-11)R_T$

## VII. SUMMARY

In this paper we have analyzed the effect of the long-range interaction in the transport through ordered and disordered nanoparticle arrays. To this end we have introduced a model which allows a discussion of the relevant quantities in determining these transport properties. We have introduced the concept of polarization potential drop, which results from the interaction between charges at the electrodes and at the islands. In the model used we take into account that electrodes are not ideal voltage sources. Their potential fluctuates in response to tunnel-

ing processes (but its effect in the numerical results is very small).

We have studied how the proximity of the nanoparticles modifies the  $1/r$ -interaction due to screening. To determine this screening we have developed two methods which allow us to calculate the inverse capacitance matrix of the system under study, see Appendix I. As discussed in Appendix II, and shown in Fig. 8(a), for the case of metallic nanoparticles, here considered, the effect of screening starts to be relevant when  $d/r^{isl} \sim 1-2$ , there is no divergency in the value of  $C_{ii}^{-1}$  at small  $d/r^{isl}$  values, but capacitance values and their inverses saturate at finite values. As discussed previously by Matsuoka and Likharev<sup>57</sup> for cylindrical nanoparticles, the interaction between charges is reduced only when the nanoparticles are very close, at larger distances the interaction increases and approaches the  $1/r$  law from above, resulting in a bump in the interaction potential as compared to Coulomb law, see Fig. 8(b). We have related this anti-screening effect with the dipolar charges induced in the conductors.

Long-range interactions screen the disorder potential and induce correlations between the values of  $\phi_i^{dis}$  at different islands. These correlations are related to, but smaller than the inverse capacitance matrix elements. The distribution of the island and junction potentials is modified in comparison to the one found for onsite interactions. These effects are discussed in section III, and are shown in Figs. 1 and 2.

As discussed in section IV, as in the onsite case, the current is blocked up to a threshold value  $V_T$ . This threshold value is independent of the resistances of the junctions. In clean arrays,  $V_T$  is the minimum voltage that allows the creation of an electron-hole pair, see Figs. 3(a) and (b). This behavior is opposite to the one found in the onsite case where a charge gradient at the junctions has to be created to allow the flow of current. With long-range interactions, the polarization potential drop across the array creates a potential gradient which facilitates charge flow. In the disordered case, two effects compete that can increase or decrease the threshold voltage compared to the clean case. Charge accumulation can be induced by up-steps in the disorder potential, increasing  $V_T$ , and the disorder potential distribution can reduce the energy to create an electron-hole pair decreasing it. The latest effect dominates for small  $d/r^{isl}$ , see Fig. 3(c).

The current varies linearly with respect voltage close to threshold, in the bottle-neck regime. This is discussed in section V and plotted in Fig. 4. The slope depends, as the threshold voltage does on the polarization potential drop, and also on the resistance of the bottle-neck junction. At intermediate voltages, we find steps in the current, but these are smoothed as compared to the onsite case, see Fig. 5(a) and (b). Contrary to the onsite case, due to the interaction between the charges in different islands the width of the steps is not fixed. A linear dependence of current on voltage is recovered for large

biases, but as in the onsite case, current extrapolates to zero at a finite offset voltage (Fig. 5(c) and (d)). The offset voltage is given by the sum of the excitonic energies of all the junctions, and its value depends on the range of the interaction, but as in the case of onsite interactions the slope of the current is given by the sum of the resistances in series and is independent of  $d/r^{isl}$ .

The voltage drop through the array close to threshold, reflects the polarization contribution  $\Lambda_i^\alpha$  due to the electrodes, as shown in Fig. 6. In the onsite case, the potential drop in this bottle-neck regime was due to the charge accumulation at the islands, necessary to create a potential gradient through the array.

Shown in Fig. 7, at intermediate voltages an oscillatory voltage drop through the array, similar to the one found for short range interactions is found for large values of  $d/r^{isl}$ . For small  $d/r^{isl}$  there is some remnant of this behavior but the amplitude of the oscillations can vanish while still being in the first step of the Coulomb staircase, which is not well defined in this case. At large voltages, the potential drop is analogous to the one found in the onsite case.

In conclusion, we have found that the long-range character of the interaction modifies the I-V characteristics of one-dimensional arrays for both ordered and disordered arrays. This modification is greatly due to the finite polarization potential drop at the bulk junctions, due to the interactions between charges at the islands and at the electrodes. Differences in transport as a function of the range of the interaction are larger at low voltages. In both the long-range and onsite cases the current is blocked up to a threshold voltage  $V_T$  and the current depends linearly on for very small  $(V - V_T)$ , but the value of both  $V_T$  and the slope of the current are different in both cases, as the mechanism to create a potential gradient through the array differs. At high voltages, for given values of the excitonic energies the transport in both cases is analogous.

## VIII. APPENDIX I: METHODS TO COMPUTE THE CAPACITANCE MATRIX

In this appendix we discuss the two methods that we have used to calculate the interaction strength  $C_{\alpha\beta}^{-1}$ . In the first one we determine the capacitance matrix using the method of images. This is an iterative method which a priori can be used to determine the capacitance matrix  $C_{\alpha\beta}$  for any geometric configuration of spheres, so it is valid also for two-dimensional arrays, for example. Although the algorithm for generating images is straightforward, the number of images required to calculate  $C_{\alpha\beta}$  makes the numerical implementation of this technique nontrivial. While computer memory problems can be solved, the computation time is too large to tackle those cases with very large arrays and electrodes and small distance between conductors. On the other hand, the capacitance matrix is calculated to a given accuracy. Small

errors in  $C_{\alpha\beta}$  can be enhanced and uncontrolled in  $C_{\alpha\beta}^{-1}$ . In the second method the interaction matrix  $C_{\alpha\beta}^{-1}$  is calculated directly taking into account the symmetry of the system and the properties of spherical harmonics. It requires the inversion of a matrix which can be quite large. It is specially useful and fast for systems with azimuthal symmetry as the one considered here. Results obtained with both methods are in extremely good agreement.

### A. Image Charges Method

The method of images is based on the relation between charges and potentials in capacitively coupled conductors. The charge  $Q_\alpha$  induced on a conductor in the presence of  $K$  equipotentials at potentials  $V_\beta$  is given by the capacitance matrix  $C_{\alpha\beta}$

$$Q_\alpha = \sum_{\beta=1}^K C_{\alpha\beta} V_\beta \quad (19)$$

The inverse capacitance matrix which enters the free energy (1) is the inverse of the capacitance matrix  $C_{\alpha\beta}$ . We have calculated the capacitance matrix using some properties of spheres and the fact that the charge in a conductor  $\alpha$  produced by a unit potential in a conductor  $\beta$  is equal to the capacitance matrix element  $C_{\alpha\beta}$ . We have obtained  $C_{\alpha\beta}^{-1}$  inverting  $C_{\alpha\beta}$ . The method of images<sup>63</sup> is the placement of imaginary charges inside the spheres at positions that make the potential everywhere on the surface of the conductor equal a constant.

To determine the positions of the image charges, we exploit two properties of spheres. First, the center of the sphere is equidistant from all points on the surface of the sphere. Using this property, the surface of a sphere of radius  $R$  can be set to a potential  $V$  by placing an image at the center of the sphere of charge  $q = VR$ . Second, for every point outside a sphere there is a point inside the sphere for which the ratio of the distances between these two points and any point on the surface of the sphere is a constant. From here it follows that if a charge  $q_R$  is located at the outside point, at a distance  $d_c$  from the center, an image charge  $q_I$  placed at the inside a distance  $R^2/d_c$  from the center in the radial line, with charge

$$q_I = -q_R \frac{R}{d_c} \quad (20)$$

will set the potential to zero everywhere on the surface of the sphere. We determine the  $(N+2) \times (N+2)$  capacitance matrix, column by column, by determining the set of image charges that sets the potentials of the spheres to  $V_\alpha = \delta_{\alpha\beta}$ . The capacitance matrix elements  $C_{\alpha\beta}$  are given by the sum of all the charges in sphere  $\alpha$ . To set the potential of the  $\beta$  sphere, with radius  $R_\beta$  to one, we place a charge with magnitude  $R_\beta$  at the center of this sphere  $x_\beta$ . The remaining spheres are grounded by

placing images inside each sphere with charges

$$q_\nu = -\frac{R_\nu q^{old}}{|x_{qold} - x_\nu|} \quad (21)$$

at positions

$$x_{q_\nu} = x_\nu + \frac{R_\nu^2}{x_{qold} - x_\nu}. \quad (22)$$

Here  $q^{old}$  and  $x_{qold}$  are the value and the position of the charge which creates the inhomogeneous potential that we want to compensate and  $R_\nu$  and  $x_\nu$  are the radius and position of the center of the sphere to which we add the image charge  $q_\nu$ . These image charges are added to all the spheres except the one in which  $qold$  is placed. The charges that have been added generate new inhomogeneous potentials at the rest of the spheres and have to be compensated following the same method. This process repeats iteratively for all the charges added to all the spheres. During each iteration  $n$ , the number of new images required to compensate the potential of the other spheres approximately equals  $(N+1)^n$ . We eliminate some of the images by discarding images with a magnitude that is smaller than a suitable cutoff value,  $q_{cutoff}$ . We required  $q_{cutoff}$  to be small enough that the relative differences between the matrix elements generated with the cutoff value  $q_{cutoff}$  and by a larger cutoff value  $q'_{cutoff} = 10q_{cutoff}$  are less than one percent.

## B. High-order multipoles method

Following Wehrli *et al*<sup>64</sup>, the energy of the system, given by (1) can be rewritten in terms of the higher-order multipolar charges induced by the charges on the conductors as

$$F = \frac{1}{2} \sum_{\alpha, \beta, l, m, l', m'} Q_{l, m}^{\alpha*} G_{l, m, l', m'}^{\alpha\beta} Q_{l', m'}^\beta. \quad (23)$$

Here Greek indices denote the conductors,  $l$  and  $l'$  denote the order of the multipole, and  $m = -l, \dots, l$  and  $m' = -l', \dots, l'$  denote the azimuthal number. This matrix  $G$  is hermitian with respect to the exchange of  $\alpha, l, m$  and  $\beta, l', m'$ . Using the linear response form for the induced multipoles, the higher-order multipolar charges,  $Q_{l, m}^\alpha$ , can be expressed in terms of the (monopolar) charges on the conductors  $Q_\gamma = Q_{00}^\gamma$ , as

$$Q_{l, m}^\alpha = \sum_\gamma \Gamma_{l, m}^{\alpha\gamma} Q_\gamma. \quad (24)$$

Substituting (24) into (23) and comparing it with (1), the inverse capacitance matrix can be expressed as

$$C_{\gamma\eta}^{-1} = \sum_{l, m, l', m', \alpha, \beta} G_{l, m, l', m'}^{\alpha\beta} \Gamma_{l, m}^{\alpha\gamma*} \Gamma_{l', m'}^{\beta\eta}. \quad (25)$$

The multipolar charge induced is the one which minimizes the energy. Separating the monopolar contribution ( $l, m = 0$ ) in the expression of the free energy, and minimizing the latter with respect to  $Q_{l, m}^\alpha$ , we obtain

$$\mathbf{Q}_A = -\hat{G}_{AB}^{-1} \hat{G}_{B0} \mathbf{Q}_0. \quad (26)$$

Here  $A = l, m$  and  $l \neq 0$ , correspondingly  $B$ , and the equation is written in vectorial and matrix notation. Once this expression is substituted in the free energy, the inverse capacitance can be written in terms of the  $\hat{G}$  matrices

$$\hat{C}^{-1} = \hat{G}_{00} - \hat{G}_{0A} \hat{G}_{AB}^{-1} \hat{G}_{B0} \quad (27)$$

The order of approximation in this method is the number of the highest multipoles  $l, l'$  included. Matrix  $\hat{G}_{00}$  has dimension  $N_s \times N_s$  with  $N_s$  the total number of conductors. Matrices  $\hat{G}_{0A}$  and  $\hat{G}_{B0}$  are  $N_s \times (N_s N_{totalmulti})$  and  $(N_s N_{totalmulti}) \times N_s$  respectively, and matrix  $\hat{G}_{AB}$  has dimension  $(N_s N_{totalmulti}) \times (N_s N_{totalmulti})$ .  $N_{totalmulti}$  is the maximum number of multipolar terms considered. Formally it is

$$N_{totalmulti} = \sum_{l=1, l_{max}} (2l+1) \quad (28)$$

with  $l_{max}$  the order of the maximum multipole included in the approximation. However the symmetries of the problem can help us to reduce it as the  $\hat{G}_{AB}$  elements corresponding to certain  $m_l$  can be seen to vanish by symmetry. In particular in the case of azimuthal symmetry, considered in the text, only  $m = 0$  gives non-zero values and the number of terms included can be reduced to  $N_{totalmulti} = l_{max}$ . Depending on the geometry of the conductors it can be convenient to use different number of  $l_{max}$  for different conductors. In particular in the case of an array of small islands sandwiched by two large electrodes, it is better to use a larger number of multipoles at the electrodes. Most of the cases presented here are done with  $l_{max} \sim 8$ .

The expression for  $G_{lm}^{\alpha\beta}$  follows from the decomposition of  $1/|\mathbf{a}-\mathbf{b}-\mathbf{R}|$ , with  $\mathbf{a}$ ,  $\mathbf{b}$  and  $\mathbf{R}$  three points in space and depends on the geometry of the conductors. For  $\alpha \neq \beta$

$$G_{l_1 m_1 l_2 m_2}^{\alpha\beta} = \left[ \frac{(l_1 + l_2 - m_1 - m_2)! (l_1 + l_2 - m_1 + m_2)!}{(l_1 + m_1)! (l_1 - m_1)! (l_2 + m_2)! (l_2 - m_2)!} \right]^{1/2} (-1)^{l_2 + m_2} I_{l_1 + l_2 + m_1 - m_2}(x_\beta - x_\alpha) \quad (29)$$

with  $I_{l, m}$  the irregular solid spherical harmonics

$$I_{lm}(\mathbf{r}) = \frac{1}{r^{l+1}} \sqrt{\frac{4\pi}{2l+1}} Y_{lm}(\Omega) \quad (30)$$

The sign of  $G_{l_1 m_1 l_2 m_2}^{\alpha\beta}$  depends not only on  $l_2$  and  $m_2$ , but also on the order  $\alpha\beta$  or  $\beta\alpha$  through the dependence of  $I_{l_1 + l_2 + m_1 - m_2}(x_\beta - x_\alpha)$ .



For the case of an sphere  $\alpha$  with radius  $R_\alpha$ ,  $G_{l_1, m_1, l_2, m_2}^{\alpha\alpha}$

$$G_{l_1 m_1 l_2 m_2}^{\alpha\alpha} = \delta_{m_1 m_2} \delta_{l_1 l_2} \frac{1}{R_\alpha} {}^{2l_1+1} \quad (31)$$

The case of spheres on a row is especially simple. In this case we have azimuthal symmetry what means that all terms involving  $m \neq 0$  should vanish. Thus at order  $l_{max}$  we have just  $N_{totalmulti} = l_{max}$ . This simplification allows us to go to reasonably high orders. We can eliminate the indexes  $m_1, m_2$  from the matrix  $G$ . Together with the diagonal terms  $G^{\alpha\alpha}$  calculated above, and using that

$$Y_{l0} = \sqrt{\frac{4\pi}{2l+1}} P_l(\cos\theta) \quad (32)$$

and  $P_l(1) = 1$  and  $P_l(-1) = (-1)^l$  the equations are greatly simplified. Thus

$$G_{l_1, l_2}^{\alpha\beta} = \frac{(l_1 + l_2)!}{l_1! l_2!} (-1)^{l_1} \frac{1}{r_{\alpha\beta}^{l_1 + l_2 + 1}}, \text{ if } x_\beta > x_\alpha$$

$$G_{l_1, l_2}^{\alpha\beta} = \frac{(l_1 + l_2)!}{l_1! l_2!} (-1)^{l_2} \frac{1}{r_{\alpha\beta}^{l_1 + l_2 + 1}}, \text{ if } x_\beta < x_\alpha \quad (33)$$

for  $\alpha \neq \beta$ . Here  $r_{\alpha\beta}$  is the distance between the centers of the spheres  $\alpha$  and  $\beta$ . The diagonal of  $G_{0A}$  and  $G_{A0}$  are zero and  $G_{0A}^{\alpha\beta} = G_{A0}^{\beta\alpha}$ . Note that

$$G_{00}^{\alpha\alpha} = \frac{1}{R_\alpha} \quad (34)$$

and

$$G_{00}^{\alpha\beta} = \frac{1}{r_{\alpha\beta}} \quad (35)$$

The zero-order approximation recovers our expectation for the case of far-apart spheres. The correction to the inverse capacitance due to the higher order multipoles is given by  $-\hat{G}_{0A} \hat{G}_{AB}^{-1} G_{B0}$ . As spheres come closer, higher order terms become more and more important. This is reasonable taking into account that the interaction between two multipolar charges  $Q_{l_1 m_1}^\alpha$  and  $Q_{l_2 m_2}^\beta$  decays as  $r_{\alpha\beta}^{l_1 + l_2 + 1}$ .

## IX. APPENDIX II. INTERACTION BETWEEN CHARGES AND CAPACITANCE MATRICES

When two conductors become closer together the mobile charges in their surfaces screen the interaction between the charges in them, compared to the  $1/r$  Coulomb law which describes the interaction between two isolated point-like charges. Other metallic systems in the surrounding environment contribute to this screening. It is expected that the charging energy of a sphere, or the energy to create an electron-hole pair between two islands will depend on the distance between the particles

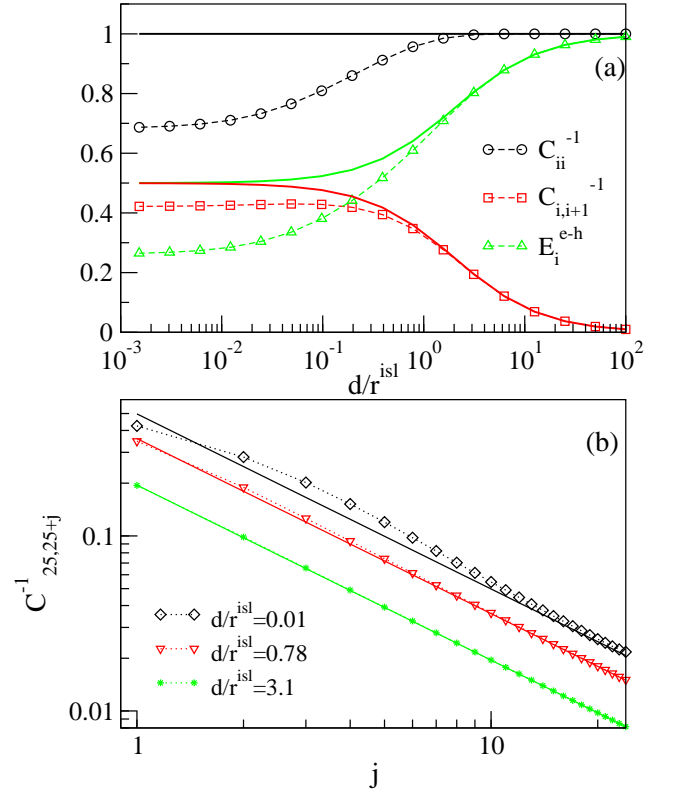


FIG. 8: (a) Island inverse capacitance  $C_{ii}^{-1}$ , nearest-neighbor interaction  $C_{i,i+1}^{-1}$  and excitonic energy, all in units of  $(C^{isl})^{-1}$ , at the center of a 50 nanoparticle array (without electrodes) as a function of the interisland separation. Solid-lines give the value obtained with a  $1/r$  interaction between charges. The effect of screening is evident for  $d/r^{isl} \leq 1 - 2$ . All the plotted quantities saturate to a finite value as  $d/r^{isl}$  vanishes. (b) Decay of the interaction potential from the center of island position for different values of  $d/r^{isl}$ . Inverse capacitances are given in units of  $(C^{isl})^{-1}$ . Solid lines correspond to an unscreened  $1/r$  law. The bump is clearly observed only for very small  $d/r^{isl}$ . It is much weaker than the one found in<sup>57</sup> and is restricted to the first nearest neighbor. For large distances the  $1/r$  law is approached from above. The effect of screening is negligible for  $d/r \sim 3$ . In (a) and (b) dashed and dotted lines are included as a guide to the eye.

in the array. In this appendix we describe the modification of the interaction due to screening and compare it with other models and calculations available in the literature.  $C_{\alpha\beta}^{-1}$  is calculated as described in Appendix I. Both methods described give the same value of  $C_{\alpha\beta}^{-1}$  to several digits when the accuracy used in the computation is good enough. Here, inverse capacitances are measured in units of  $C_{isl}^{-1}$ , the value of the inverse capacitance of a nanoparticle  $C_{ii}^{-1}$  when it is isolated. We find that the effect of screening is essentially restricted to the interactions between charges which are in the same islands or in the closest neighboring islands and only when the particles are very close  $d/r^{isl} \leq 1 - 2$ .

Three important quantities for the transport are the island inverse capacitance  $C_{ii}^{-1}$ , the nearest-neighbor interaction  $C_{i,i+1}^{-1}$  and the resulting excitonic energy  $E_i^{e-h}$ . In Fig. 8(a) we show how these quantities depend on the distance between the particles,  $d/r^{isl}$  for the case of an array with  $N = 100$  equal-sized islands, at the center of the array. The effects of screening start to be relevant for  $d/r^{isl} < 1 - 2$ . At this value  $C_{ii}^{-1}$  starts decreasing, and when  $d/r^{isl} \rightarrow 0$ , approximately at  $d/r^{isl} = 0.002$  it saturates at about 0.68 of its bare value.  $C_{i,i+1}^{-1}$  increases following a  $1/r$  law as  $d/r$  is reduced, until  $d/r^{isl} \sim 1 - 2$ . Then it decreases slightly due to the screening of the interaction, and finally it saturates at about  $d/r^{isl} = 0.1$ . At large  $d/r^{isl}$  the  $E_i^{e-h}$  starts decreasing when  $d/r^{isl}$  is reduced, according to the  $1/r$  increase of  $C_{i,i+1}^{-1}$ . For  $d/r^{isl} < 2$ , its value is affected both by the increase of  $C_{i,i+1}^{-1}$  and the decrease of  $C_{ii}^{-1}$ , at small distance is controlled by this last effect. Finally it saturates.

The modification of the distance dependent interaction in one-dimensional arrays has been previously studied for some particular island geometries. For the case of thin circular disks (with disk axis perpendicular to the array axis), Whan et al.<sup>58</sup> found that a  $1/r$  law describes well the dependence of the non-diagonal inverse capacitance matrix elements on distance and that the diagonal elements are reduced. Likharev and Matsuoka<sup>57</sup> analyzed the cases of an array of cubic islands (with inverse capacitance matrix calculated using the finite-differences software FASTCAP) and a continuum model in which the discrete periodic structure is replaced by a continuous dielectric medium. They found that the dependence of the interaction on the distance between the charges  $r$  has a crossover between a linear dependence at short distances and a  $1/r$  law at long distances. There is a bump on the interaction when compared to a  $1/r$  law. The potential approaches the  $1/r$  law from above. The interaction potential could be approximated by the expression

$$U(m) = \frac{e^2}{a} \left( \frac{\alpha}{m_0} \exp\left(\frac{-\kappa m}{m_0}\right) + \frac{1}{m} \left[ 1 - \exp\left(\frac{-\kappa m}{m_0}\right) \right] \right) \quad (36)$$

Here  $m$  is the distance in units of the array period,  $a$ ,  $m_0 = r_0/a$ , with  $r_0 = S\epsilon/\pi$  a characteristic decay length of the interaction.  $\epsilon$ , the inter-islands dielectric constant,  $S$  the junction surface and  $\kappa$  a fitting parameter with value very close to 1 and related to  $\alpha$  by

$$\alpha = \frac{2}{\kappa} - \frac{\kappa}{2} \quad (37)$$

The dependence of  $C_{i,i+j}^{-1}$  on  $j$  that we have obtained for the experimentally relevant case of an array of spherical particles is plotted in Fig. 8(b). Screening is less important for the case of spheres than for cubic islands but larger than for the thin disks analyzed by Whan *et al.*<sup>58</sup>. Compared with a  $1/r$  law, at short distance the screened interaction potential decreases and at large distances it increases. When the particles are very close,

there is a bump in the renormalization of the interaction. Only when two charges are in the same particle or at the nearest neighbor one the interaction between them decreases. In other cases the interaction increase. We have not been able to fit our results with (36). We recover the bump found by Likharev and Matsuoka<sup>57</sup>, but it is smaller than the one they observe, even when our particles are very close. We believe that the differences are due to the different geometry of the system under study.

From the decomposition of the induced screening charge in high-order multipoles discussed in previous appendix it is possible to get some insight on how does the bump appear. The correction to the inverse capacitance  $\delta C^{-1}$  due to screening is  $-\hat{G}_{0A}\hat{G}_{AB}^{-1}\hat{G}_{B0}^{-1}$ , see (27), which has the same sign as the monopole-induced multipole interaction. Thus,  $\delta C_{\alpha\beta}^{-1}$  has the same sign as the interaction of the monopolar charge in  $\alpha$  with the multipolar charge induced in all conductors by the monopolar charge in  $\beta$ . Let us restrict to dipolar order, which will be the largest contribution.  $Q_\beta$  generates dipolar charges in all the other conductors  $\gamma$ , equal to  $Q^{\gamma\beta} = \sum_\nu (G_{11}^{\nu\nu})^{-1} G_{10}^{\nu\beta} Q_\beta$  and the monopolar charge in  $\alpha$  interact with these induced charges via  $G_{01}^{\alpha\gamma}$ . Both the monopolar-dipolar interaction  $G_{01}$  and the dipolar induced charges are odd quantities with respect to position. To dipolar order, all the elements of  $G_{11}^{-1}$  are positive. The sign of the two odd quantities will control the sign of  $\delta C_{\alpha\beta}^{-1}$ .

Consider  $\delta C_{\alpha\beta}^{-1}$ , with  $0 < \alpha < \beta < N$ , the charges induced by a monopolar charge placed in  $\beta$  in conductors from 1 to  $\alpha - 1$  and from  $\alpha + 1$  to  $\beta - 1$  have the same sign, but the interaction of a monopolar charge in  $\alpha$  with them, have opposite. Thus those terms coming from the charge induced in conductors from 1 to  $\alpha - 1$  and those from conductors  $\alpha + 1$  to  $\beta - 1$  contribute to  $\delta C_{\alpha\beta}^{-1}$  with different sign. The sign of the contribution of the conductors at the right of  $\beta$  will be the same as those at the left of  $\alpha$  and both induced charge and interaction have opposite sign. As further are these conductors to  $\alpha$  and  $\beta$  the correction will be smaller. Individual contributions from each conductor  $\gamma$  will be larger when  $\alpha < \gamma < \beta$ . The contribution of the interaction term which comes from the dipoles generated in conductors between  $\alpha$  and  $\beta$  increase  $C_{\alpha\beta}^{-1}$ . Only when the contribution of the terms which decrease the inverse capacitance matrix element is able to compensate the contribution of those ones which increase it, the total change will be negative. As closer are  $\alpha$  and  $\beta$  the number of terms increasing the interaction will decrease.  $C_{\alpha\beta}^{-1}$  is expected to be smaller than the bare value, only if  $\alpha$  and  $\beta$  are very close, what results in the appearance of the bump and the anti-screening effect at intermediate and large distances.

The interaction obtained differs considerably from the one resulting from capacitive coupling only to nearest-neighbors. This form of the interaction has been used frequently in the literature, and applies when the system is coupled to a gate electrode which screens the long-



range part. The capacitance matrix has a triband form. Only  $C_{ii} = C_0 + 2C$  and  $C_{i,i\pm 1} = -C$  are finite. The inverse of  $C_{ij}$  for the case of an infinite array becomes

$$C_{ij}^{-1} = \frac{1}{C^\infty} e^{-|i-j|/\xi} \quad (38)$$

with  $\xi$  and  $C^\infty$  defined from  $C^\infty = 2Csh(\xi^{-1}) = (C_0^2 + 4CC_0)^{1/2}$ . Due to the exponential dependence  $\xi$  can be viewed as the decay length of the interaction, which increases with  $C/C_0$ . Interactions on the same island are given by  $C_{ii}^{-1} = 1/C^\infty$ . In the case of a finite array of length  $N$  this value is approached, from below, as  $N$  increases. The onsite case is recovered when  $C = 0$  and long-range interactions appear in the opposite limit  $C_0/C \rightarrow 0$ . In the later limit the interaction potential goes like

$$C_{ij}^{-1} = \frac{1}{2C} \left( \frac{N}{2} - |i-j| \right) \quad (39)$$

It decays linearly with distance. The energy to create an electron-hole pair  $E_i^{e-h} = 1/2C_{ii}^{-1} + 1/2C_{i\pm 1,i\pm 1}^{-1} - C_{i,i\pm 1}^{-1}$  remains bound and equal to  $1/(2C)$ . On the contrary, the diagonal element  $C_{ii}^{-1} = \frac{1}{4C}N$  diverges with the array size. There is not such unphysical divergence in  $C_{ii}^{-1}$  with the array size in our model.

To analyze the transport properties the array is sandwiched between two electrodes, much larger than each of the nanoparticles. To this end we consider a one-dimensional array of  $N$  nanoparticles placed in between two large spheres, with radius  $R$ , which play the role of the leads. The large size ensures large screening and that  $C_{00}^{-1}$  and  $C_{N+1,N+1}^{-1}$  are much smaller than the islands  $C_{ii}^{-1}$ . The spherical shape greatly simplifies the

calculations of the inverse capacitance matrix. The interaction between the charges at the islands and those at the electrodes and the inverse capacitance elements of the electrodes determine  $\lambda_i^\alpha$  and  $\Lambda_i^\alpha$ , which control the polarization voltage drop through the array and to a large extent the current flow at small voltages, see Figs. 6(a) and (b).

For the size of the electrodes used in the text,  $R \sim 50 - 100r^{isl}$ , the inverse capacitance of the islands close to the electrodes is slightly reduced compared to those at the center, except for very small  $d/r^{isl}$ . For small  $d/r^{isl}$  the inverse capacitance of islands at the center of the array is almost insensitive to the presence of the electrodes. If the electrodes are much larger the dependence of the inverse capacitance matrix elements with the size of the electrodes can become non-monotonous. This behavior, like the one found for small  $d/r^{isl}$  is most probably associated to the spherical shape chosen to model the electrodes.

We thank S. Wehrli for useful discussions. Financial support from the Swiss National Foundation, NCCR MaNEP of the Swiss National Fonds, the Spanish Science and Education Ministry through Ramón y Cajal contract FPI fellowship and grant No. FIS2005-05478-C02-02 and the Dirección General de Universidades e Investigación de la Consejería de Educación de la Comunidad de Madrid and CSIC through Grant No. 200550M136 is gratefully acknowledged. Work at UT Austin was supported by the Welch Foundation, by the NSF under grant DMR-0606489 and by the ARO under grant W911NF-07-1-0439.

---

\* Electronic address: leni@icmm.csic.es

- <sup>1</sup> R.L. Whetten, J.T. Khoury, M.M. Alvarez, S. Murthy, I. Vezmar, Z.L. Wang, P.W. Stephens, C.L. Cleveland, W.D. Luedtke and U. Landman, *Adv. Mater.* **8**, 428 (1996).
- <sup>2</sup> C.P. Collier, R.J. Saykally, J.J. Shiang, S.E. Henrichs, J.R. Heath, *Science* **277**, 1978 (1997). G. Markovich, C. P. Collier, S.E. Henrichs, F. Remacle, R.D. Levine and J.R. Heath, *Acc. Chem. Res.* **32**, 415 (1999).
- <sup>3</sup> R. Parthasarathy, X.-M. Lin and H. M. Jaeger, *Phys. Rev. Lett.* **87**, 186807 (2001).
- <sup>4</sup> J.D. Le, Y. Pinto, N.C. Seeman, K. Musier-Forsyth, T.A. Taton and R.A. Kiehl, *Nanoletters* **4**, 2343 (2004).
- <sup>5</sup> Y. Lin, A. Böker, J. He, K. Sill, H. Xiang, C. Abetz, X. Li, J. Wang, T. Emrick, S. Long, Q. Wang, A. Balazs and T.P. Russell, *Nature* **434**, 55 (2005).
- <sup>6</sup> K. Elteto, X.-M. Lin and H.M. Jaeger, *Phys. Rev. B* **71**, 205412 (2005).
- <sup>7</sup> J. Zhang, Y. Liu, Y. Ke and H. Yan, *Nanoletters* **6**, 248 (2006).
- <sup>8</sup> T.P. Bigioni, X.-M. Lin, T.T. Nguyen, E.I. Corwin, T.A. Witten and H. M. Jaeger, *Nature Materials* **5**, 265 (2006).

- <sup>9</sup> J. Liao, L. Bernard, M. Langer, C. Schönenberger and M. Calame, *Adv. Mater.* **18**, 2803 (2006). (ojo comprobar si es 2803 o 2444).
- <sup>10</sup> S.S. Mark, M. Bergkvist, X. Yang, L.M. Teixeira, P. Bhatnagar, E. R. Angert and C.A. Batt, *Langmuir* **22**, 3763 (2006).
- <sup>11</sup> C.B. Murray, C.R. Kagan and M.G. Bawendi, *Science* **270**, 1335 (1995).
- <sup>12</sup> D.V. Talapin, E.V. Shevchenko, A. Kornowski, N. Gaponik, M. Haase, A.L. Rogach and H. Weller, *Adv. Mater.* **13**, 1868 (2001).
- <sup>13</sup> N.Y. Morgan, C.A. Leatherdale, M. Drndić, M.V. Jarosz, M.A. Kastner and M. Bawendi, *Phys. Rev. B* **66**, 075339 (2002). V.J. Porter, t. Mentzel, S. Charpentier, M.A. Kastner and M.G. Bawendi, *Phys. Rev. B* **73**, 155303 (2006).
- <sup>14</sup> D. Yu, c. Wang, B.L. Wehrenberg and P. Guyot-Sionnest, *Phys. Rev. Lett.* **92**, 216802 (2004).
- <sup>15</sup> H. Romero and M. Drndić, *Phys. Rev. Lett.* **95**, 156801 (2005).
- <sup>16</sup> T. Feng, H. Yu, M. Dicken, J.R. Heath and H.A. Atwater, *App. Phys. Lett.* **86**, 033103 (2005).

- <sup>17</sup> S. Sun, C.B. Murray, D. Weller, L. Folks and A. Moser, *Science* **287**, 1989 (2000).
- <sup>18</sup> C.T. Black, C.B. Murray, R.L. Sandstrom and S. Sun, *Science* **290**, 1131 (2000)
- <sup>19</sup> V. F. Puentes, P. Gorostiza, D.M. Aruguete, N.G. Bastus and A.P. Alivisatos, *Nature Materials* **3**, 263 (2004).
- <sup>20</sup> F.X. Redl, K.-S. Cho, C.B. Murray and S. O'Brien, *Nature (London)* **423**, 968 (2003).
- <sup>21</sup> A.E. Saunders and B. A. Korgel, *Chem. Phys. Chem.* **6**, 61 (2005).
- <sup>22</sup> E.V. Schevchenko, C.V. Talapin, N.A. Kotov, S. O'Brien and C.B. Murray, *Nature (London)* **439**, 55 (2006).
- <sup>23</sup> *Single Charge Tunneling, NATO ASI Series, Vol B*, 294, eds. H. Grabert and M.H. Devoret., New York, Plenum Press 1992.
- <sup>24</sup> P. Sheng and B. Abeles, *Phys. Rev. Lett.* **28**, 34 (1972). P. Sheng, B. Abeles and Y. Arie, *Phys. Rev. Lett.* **31**, 44 (1973). J.S. Helman and B. Abeles, *Phys. Rev. Lett.* **37**, 1429 (1976).
- <sup>25</sup> J.J. Shiang, J.R. Heath, C.P. Collier and R.J. Saykally, *J. Phys. Chem. B* **102**, 3425 (1998).
- <sup>26</sup> S.-H. Kim, G. Medeiros-Ribeiro, D.A.A. Ohlberg, R.S. Williams and J.R. Heath, *J. Phys. Chem. B* **103**, 10341 (1999). J.F. Sampaio, K.C. Beverly and J.R. Heath, *J. Phys. Chem. B*, **105**, 8797 (2001)
- <sup>27</sup> I.S. Weitz, J.L. Sample, R.Ries, E.M. Spain and J.R. Heath, *J. Phys. Chem B* **104**, 4288 (2000).
- <sup>28</sup> B.M. Quinn, I. Prieto, S. K. Haram and A.J. Bard, *J. Phys. Chem. B* **105**, 7474 (2001).
- <sup>29</sup> R.C. Doty, H. Yu, C.K. Shih and B.A. Korgel, *J. Phys. Chem. B* **105**, 8291 (2001).
- <sup>30</sup> A. Courty, A. Mermet, P.A. Albouy, E. Duval and M.P. Pileni, *Nature Materials* **4**, 395 (2005).
- <sup>31</sup> M.G. Ancona, W. Kruppa, R.W. Rendell, A.W. Snow, D. Park and J.B. Boos, *Phys. Rev. B* **64**, 033408 (2001).
- <sup>32</sup> A. Bezryadin, R.M. Westervelt, and M. Tinkham, *App. Phys. Lett.* **74**, 2699 (1999).
- <sup>33</sup> N.S. Bakhalov, G.S. Kazacha, K.K. Likharev and S.I. Serdyukova, *Sov. Phys. JETP* **68**, 581 (1989).
- <sup>34</sup> A.A. Middleton and N.S. Wingreen, *Phys. Rev. Lett.* **71**, 3198 (1993).
- <sup>35</sup> K.A. Matsuoka and K.K. Likharev, *Phys. Rev. B* **57**, 15613 (1998). D.M. Kaplan, V.A. Sverdlov and K.K. Likharev, *cond-mat/0303477*.
- <sup>36</sup> M.Shin, S. Lee, K.W. Park and E.H. Lee, *Phys. Rev. Lett.* **80**, 5774 (1998).
- <sup>37</sup> M. Stopa *Phys. Rev. B* **64**, 193315 (2001).
- <sup>38</sup> D.M. Kaplan, V.A. Sverdlov and K.K. Likharev, *Phys. Rev. B* **65**, 193309 (2002).
- <sup>39</sup> D.A. Kaplan, V.A. Sverdlov and K.K. Likharev, *Phys. Rev. B* **68**, 045321 (2003).
- <sup>40</sup> Y.A. Kinkhabwala, V.A. Sverdlov, K.K. Likharev, *J. of Phys. Condens. Matter* **18** 2013 (2006).
- <sup>41</sup> S. Semrau, H. Schoeller and W. Wenzel, *Phys. Rev. B* **72**, 205443 (2005).
- <sup>42</sup> R.Kotliar and S. Das Sarma, *Superlatt. and Microst.* **20**, 641 (1996).
- <sup>43</sup> I.S. Beloborodov, A.V. Lopatin, V.M. Vinokur and K.B. Efetov, *Rev. Mod. Phys.* **79**, 469 (2007). I.S. Beloborodov, A. Glatz and V.M. Vinokur, *Phys. Rev. B* **75**, 052302 (2007). T.B. Tran, I.S. Beloborodov, X.M. Lin, T.P. Bigioni, V.M. Vinokur and H.M. Jaeger, *Phys. Rev. Lett.* **95**, 076806 (2005).
- <sup>44</sup> A. Atland, L. Glazman, A. Kamenev, *Phys. Rev. Lett.* **92**, 026801 (2004). J.S. Meyer, A. Kamenev and L.I. Glazman, *Phys. Rev. B* **70**, 045310 (2004).
- <sup>45</sup> Y.L. Loh, V. Tripathi and M. Turlakov, *Phys. Rev. B* **72**, 233404 (2005).
- <sup>46</sup> K.B. Efetov and A. Tschersich, *Europhys. Lett.* **59**, 114 (2002).
- <sup>47</sup> J. Zhang and B.I. Shklovskii, *Phys. Rev. B* **70**, 115317 (2004).
- <sup>48</sup> R. Parthasarathy, X.-M. Lin, K. Elteto, T.F. Rosenbaum and H.M. Jaeger, *Phys. Rev. Lett.* **92**, 076801 (2004). K. Elteto, E. G. Antonyan, T. T. Nguyen, and H. M. Jaeger, *Phys. Rev. B* **71**, 064206 (2005).
- <sup>49</sup> K.C. Beverly, J.F. Sampaio and J.R. Heath, *J. Phys. Chem B* **106**, 2131 (2002). F. Remacle, C.P. Collier, G. Markovich, J.R. Heath, U. Banin, R.D. Levine *J. Phys. Chem B* **102**, 7727 (1998). F. Remacle, K.C. Beverly, J.R. Heath and R.D. Levine, *J. Phys. Chem B* **106** 4116 (2002).
- <sup>50</sup> A.S. Cordan, A. Goltzené, Y. Hervé, M. Mejías, C. Vieu and H. Launois, *Jour. of App. Phys.* **84**, 3756 (1998). A. Pépin, C. Vieu, M. Mejias, Y. Jin, F. Carcenac, J. Gieraz, C. David, L. Couraud, A. S. Cordan, Y. Leroy and A. Goltzené, *App. Phys. Lett.* **74**, 3047 (1999). A.S. Cordan, Y. Leroy, A. Goltzené, A. Pepin, C. Vieu, M. Mejias and H. Launois, *Jour. of App. Phys.* **87** 345 (2000). Y. Leroy, A. S. Cordan and A. Goltzené, *Jour. of App. Phys.* **90** 953 (2001).
- <sup>51</sup> G.Y. Hu and R.F. O'Connell, *Phys. Rev. B* **49**, 16773 (1994).
- <sup>52</sup> J.A. Melsen, U. Hanke, H.O. Müller and K.A. Chao, *Phys. Rev. B* **55**, 10638 (1997).
- <sup>53</sup> C.A. Berven and M.N. Wybourne, *App. Phys. Lett.* **78**, 3893 (2001).
- <sup>54</sup> S. Jha and A.A. Middleton, *cond-mat/0511094*
- <sup>55</sup> C. Kurdak, A.J. Rimberg, T.R. Ho and J. Clarke, *Phys. Rev. B* **57**, R6842 (1998).
- <sup>56</sup> E. Bascones, V. Estévez, J.A. Trinidad, A.H. MacDonald, *arXiv:0709.3718*
- <sup>57</sup> K.K. Likharev and K.A. Matsuoka, *Appl. Phys. Lett.* **67**, 3037 (1995).
- <sup>58</sup> C.B. Whan, J. White and T.P. Orlando, *App. Phys. Lett.* **68**, 2996 (1996).
- <sup>59</sup> C.Reichhardt and C.J. O. Reichhardt, *Phys. Rev. Lett.* **90**, 046802 (2003).
- <sup>60</sup> Y. Xue and M.A. Ratner, *Phys. Rev. B* **68**, 235410 (2003).
- <sup>61</sup> N.S.Bakhalov, G.S. Kazacha, K.K. Likharev and S.I. Serdyukova, *Physica B* **173**, 319 (1991).
- <sup>62</sup> U. Geigenmüller and G. Schön, *Europhys. Lett.* **10**, 765 (1989).
- <sup>63</sup> W.R. Smythe *Static and Dynamic Electricity* (McGraw-Hill, New York, 1950).
- <sup>64</sup> S. Wehrli, E. Koch and M. Sigrist, *Phys. Rev. B* **68**, 115412 (2003).